A Variational Approach for Physically Based Image Interpolation Across Boundaries

Matthias Klinger

Abstract In this contribution we present an optimal control approach for physics-based optical flow estimation and image interpolation. The aim of the developed process is to identify appropriate boundary data of an underlying physical model describing the transport field, which reason the movement of an initial brightness distribution. Thereby, the flow field as solution of the time-dependent non-linear Navier-Stokes equations is coupled to a transport dominant convection-diffusion equation describing the brightness intensity. Thus, we have to deal with a weakly coupled PDE system as state equation of a PDE constrained optimisation problem. The data is given in form of consecutive images, with a sparse temporal resolution, representing the brightness distribution at different time points. We will present the mathematical theory of the resulting optimisation problem, which is based on a Robin-type boundary control. We describe the numerical solution process and present by means of synthetical test cases the functionality of the method. Finally we discuss the application of multiple shooting techniques for the considered problem, since we observed that the employed Newton-type method is very sensitive with respect to the chosen initial value.

1 Introduction

In many fields of research scientists are interested in fluid motion, e.g. weather forecast, circulation around obstacles, microfluidic flows. However, to evaluate accurate flow fields is often a hard task, regardless if we use measurement techniques to document an observed flow or numerical modelling to simulate a similar flow situation. A common methodology to document a fluid motion is to observe the movement of a passive tracer in a given fluid flow by consecutive images. These images represent a spatial and temporal discretisation of the evolution of a brightness distribution given by a camera apparatus, which detects light signals transmitting through the transparent fluid and the light absorbing passive tracer.

M. Klinger (✉)
Institut für Angewandte Mathematik, Im Neuenheimer Feld 294, 69120 Heidelberg, Germany
e-mail: matthias.klinger@iwr.uni-heidelberg.de

T. Carraro et al. (eds.), *Multiple Shooting and Time Domain Decomposition Methods*, Contributions in Mathematical and Computational Sciences 9,
DOI 10.1007/978-3-319-23321-5_13

The transport of a brightness value in the image domain is caused by a velocity field, which is called the optical flow. In some situations the optical flow is closely connected to the underlying physical flow. Heitz et al. [20] for example mention that there exists a straightforward connection between the optical flow and the fluid flow of a laser sheet visualisation of a two dimensional incompressible flow, when the laser sheet is perfectly aligned with the flow. Thus the optical flow $\mathbf{w}$ is proportional to the velocity $\mathbf{u}$ and satisfies a convection-diffusion equation. This connection between optical flow and fluid flow can also be assumed for the observation of three dimensional flows by two dimensional images, as long as the flow in z direction is negligible. However, the optical flow field $\mathbf{w}$ serves then only as an approximation of the planar flow field.

Hence, it is a good opportunity to work with optical flow estimation techniques to obtain approximations of fluid flow fields. Approaches toward this direction are already presented in the literature, as for example in the mentioned article of Heitz et al. [20]. Another approach basing on the reformulation of the optical flow functional by means of the underlying flow model was considered by Nakajima et al. [29]. Another promising class of approaches was presented by Ruhnau and coworkers [35–37], who regularised the classical Horn and Schunck cost functional (cf. Horn et al. [22]) by applying physical models as PDE side condition in the optimisation framework.

Especially, for environmental sciences this technique is attractive for the investigation of local wind systems in areas where a dense grid of measurement stations is unavailable, but a tracer is transported in the atmosphere, which can be observed by satellite remote sensing. For example Héas et al. [19] and Papadakis et al. [32] considered the estimation of wind field information from satellite image sequences observing cloud formations by image processing approaches. Another example for environmental fluid flows is the movement of dust aerosols in northern Africa in the Sahara desert. The measurements of the aerosol density in a certain area on the earths surface at different time points, obtained by an instrument installed on a geosynchronous satellite lead to a sequence of brightness distributions of a passive tracer, the aerosols, which is transported by an optical flow field, which we assume to be a approximation of the planar flow field in the ground-based atmospheric layers. First attempts to use this image sequences to obtain these optical flow fields were presented in the work of Bachl et al. [1, 2].

However, we aim to introduce a novel approach for physical-based fluid flow estimation from observations of a passive tracer by combining the single features of the above mentioned techniques in one approach, which place the emphasis on the coupling of a high fidelity physical flow model, namely the incompressible, nonlinear and time-dependent Navier-Stokes equations, to the optical flow equation by applying so called boundary controls. Then our focus is on the theoretical justification and the numerical realisation of the method. Furthermore, we are interested in the quality of the reconstructed underlying transport field by our approach. Unfortunately, the mentioned example of a real world application has too many complications (e.g. measurement errors, model uncertainties, occlusions, varying illumination in the images) to tackle them all at the same time. Furthermore,

appropriate reference data for a qualitative comparison of our results are not available. Hence, we will consider a prototypical example with synthetic images and some simplifications to present our approach, which employs beside the image information also informations about the physical flow model and allows also movement across the image domain boundaries, since images often represent only an aperture of the real scenery.

Therefore, we assume that we observe a plane motion described by the time-dependent (Navier-) Stokes equations, which transport a brightness distribution $I(\mathbf{x}, t)$ due to the following system of equations

$$\begin{aligned} \partial_t I - \varepsilon \Delta I + \mathbf{u} \cdot \nabla I &= 0, \\ \partial_t u - \nu \Delta \mathbf{u} + \mathbf{u} \cdot \nabla \mathbf{u} + \nabla p &= \mathbf{f}, \qquad \text{in } \Omega \times (0, T], \\ \nabla \cdot \mathbf{u} &= 0, \end{aligned} \tag{1}$$

with appropriate initial and boundary data. The image sequences are then obtained by setting $\mathscr{I}_k = I(\mathbf{x}, t_k)$ at discrete times t_k.

Figures 1, 2 and 3 show three examples of such artificial image sequences. The first two sequences are obtained with very simple flow fields but with flow across the boundaries. In the third test case we observe a flow field which exhibits the time-dependent character of the system (1). Our aim is then to identify the underlying flow fields and the movement of the (bulb) signal. For this purpose we present an optimisation problem with system (1) as PDE constraint. Thus, our methodology can be interpreted as an optimal control problem with parabolic PDE constraints. Such parabolic optimal control problems and their numerical treatment are widely

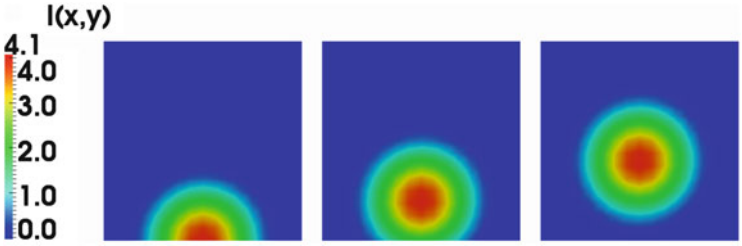

Fig. 1 *Left*: $\mathscr{I}_1$ at $t = 0$. *Middle*: $\mathscr{I}_2$ at $t = 0.1$. *Right*: $\mathscr{I}_3$ at $t = 0.2$. The transport field is given by $\mathbf{u} = (2, 0)^T$

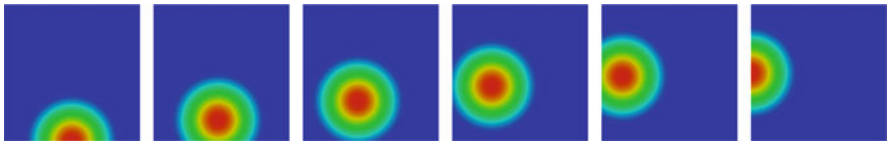

Fig. 2 $(\mathscr{I}_k)_{k=1}^6$ at the time points $t_k = 0.04(k-1)$. The transport field is $\mathbf{u} = \kappa(-y, x)^T$ with $\kappa = \frac{5}{2}\pi$

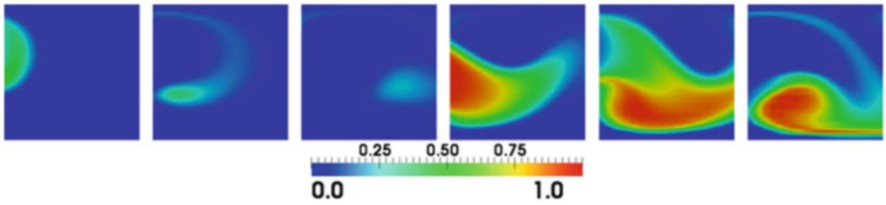

Fig. 3 $(\mathscr{I}_k)_{k=1}^6$ at six different time points transported by a time-dependent solution of the Navier-Stokes equations $\mathbf{u}(\mathbf{x}, t)$

discussed in the literature. We will mention a few example which are related to the presented topics in this article. For example Kolmbauer et al. [26] present an approach for time-periodic eddy current optimal control problems. Pearson et al. [33] consider the numerical treatment of optimal control problems constrained by convection-reaction problems while the article of Stoll et al. [38] considers the time-dependent Stokes equation as side condition. Finally Gunzburger et al. [18] discuss the use of space-time adaptive methods for optimal control problems with parabolic evolution equations as side condition.

The article is organised in the following way. At first we describe variational optical flow estimation techniques for the above mentioned synthetic image sequences. Furthermore we describe their enhancement to optimal control problems. Then we enhance the techniques to formulations which can even deal with flows across the boundaries. Afterwards we discuss the mathematical theory for the presented approach before we talk about the numerical techniques we need for a solution of the presented approach. The sixth section is devoted to the presentation of some numerical results for the mentioned artificial sequences. In the final section we discuss the reformulation of our abstract problem as temporal boundary value problem and the possible advantages of applying a multiple shooting method.

2 Physics-Based Optical Flow Equation

In the following $\Omega \subset \mathbb{R}^2$ denotes the image domain, which is in general a rectangle $\Omega = (0, a) \times (0, b)$. The brightness function is given by

$$I : \Omega \times [0, T] \to \mathbb{R}^+, \qquad \{\mathbf{x}, t\} \mapsto I(\mathbf{x}, t).$$

Our observations, the images, are spatial and temporal discretisations of $I(\mathbf{x}, t)$:

$$\mathscr{I}(i, j, k) = I(\mathbf{x}_{ij}, t_k)$$

on a certain space-time grid. However we assume throughout the article that the spatial discretisation is fine, while the temporal discretisation is coarse, so that the data is given by a temporally discrete sequence

$$(\mathscr{I}_k)_{k=1}^N = (I(\mathbf{x}, t_k))_{k=1}^N.$$

We consider throughout the article a two-dimensional incompressible flow with the field $\mathbf{u} = (u, v)^T$. This flow field satisfies the two-dimensional non-stationary Navier-Stokes equations

$$\begin{aligned} \partial_t \mathbf{u} - \nu \Delta \mathbf{u} + \mathbf{u} \cdot \nabla \mathbf{u} + \nabla p &= \mathbf{f} \qquad \text{in } \Omega \times (0, T] \\ \nabla \cdot \mathbf{u} &= 0 \qquad \text{in } \Omega \times (0, T] \end{aligned}$$

for appropriate initial values and boundary data. Since we do not consider a real world application we conjecture $\mathbf{w} = \mathbf{u}$.

Remark 1 (Relation Between Optical Flow and Fluid Flow) As we already mentioned in the introduction their is a close relationship between the optical flow in an image sequence and the fluid flow, which is documented by these images observing the movement of a passive tracer. For a detailed description of this relationship we refer the interested reader to Sect. 2.1 of Heitz et al. [20]. Especially, for laser sheet visualisation of two-dimensional incompressible flows the connection between optical and fluid flow is straightforward, as long as the laser sheet is aligned with the flow field.

The brightness intensity function $I(\mathbf{x}, t)$ fulfills then the physics-based optical flow equation

$$\partial_t I + \mathbf{u} \cdot \nabla I = \varepsilon \Delta I \qquad \text{in } \Omega \times (0, T]$$

with certain boundary conditions and an appropriate initial condition.

The coupled system of Eq. (1) describes then the evolution of an initial brightness distribution $\mathscr{I}^0(\mathbf{x})$. For further considerations we assume that no domain forces cause the flow in the image domain, which means $\mathbf{f} = 0$. Thus the boundary conditions describe the flow scenario completely.

The aim of our work is to describe a method which recovers appropriate boundary conditions for the flow field and the connected brightness function only by the following available information:

(a) A temporal sparse image sequence: $(\mathscr{I}_k)_{k=1}^N$,
(b) Model parameters: ε and ν,
(c) An estimate for the initial flow field: $\mathbf{u}^0$.

3 Optimisation for Physics-Based Optical Flow

The recovering of appropriate boundary conditions is realised by a PDE constrained optimisation problem. First ideas towards this direction, especially in the image processing framework, are given in the work of Borzi et al. [8], Chen et al. [13] and Klinger [25]. We start with the definition of the optimisation problem.

Definition 1 Find $q_I \in Q_I$, $\mathbf{q_u} \in Q_\mathbf{u}$ and $(\mathbf{u}, p, I) \in V_\mathbf{u} \times V_p \times V_I$ so that the functional

$$J(\{q_I, \mathbf{q_u}\}, I) = \frac{1}{2}\sum_{k=1}^{N} \|I(t_k) - \mathscr{I}_k\|_2^2 + \frac{\alpha_1}{2}\int_0^T \|q_I(t)\|_{Q_I}^2 dt + \frac{\alpha_2}{2}\int_0^T \|q_\mathbf{u}(t)\|_{Q_\mathbf{u}}^2 dt$$

is minimised subject to an appropriate weak formulation of system (1), with $\mathbf{f} = 0$, $I(0) = \mathscr{I}_1$ and $\mathbf{u}(0) = \mathbf{u}^0$ and so called control functions $\mathbf{q_u}$ and q_I for I and $\mathbf{u}$ on the boundary.

The choices of $Q_\mathbf{u}$, Q_I and the type of boundary conditions are crucial for the well-posedness of this optimisation problem as well as for the computational realisation of the problem. We discuss a promising compromise in the next section.

3.1 Treatment of the Boundary Control Formulation

The first idea is to use Dirichlet controls

$$\begin{aligned} I &= q_I && \text{on } \partial\Omega \times (0,T] \\ \mathbf{u} &= \mathbf{q_u} && \text{on } \partial\Omega \times (0,T], \end{aligned} \tag{2}$$

where we have to choose appropriate control spaces Q_I and $Q_\mathbf{u}$. For the existence theory of solutions of the presented optimisation problem a main ingredient is the existence theory of the state equation. In our case for the coupled system (1). This system consists of a convection-diffusion equation, which is weakly coupled to the incompressible Navier-Stokes equations. Both are parabolic PDEs. The natural choice of functions to prescribe Dirichlet boundaries for parabolic PDEs is the space $H^{\frac{1}{2}}(\partial\Omega)$. This space is defined in the following way

$$H^{\frac{1}{2}}(\partial\Omega) = \{\varphi \in L^2(\partial\Omega) : \exists \omega \in H^1(\Omega),\ \varphi = \omega|_{\partial\Omega}\},$$

tributing to the fact, that L^2-functions on the boundary exist which have no H^1-extensions to the interior of the domain.

However, the implementation of an appropriate norm for this space in the cost functional is complicated. One way of doing this was suggested by Of et al. [31], by defining the semi-norm:

$$|q|^2_{H^{\frac{1}{2}}(\partial\Omega)} = \langle \mathscr{S} q, q \rangle$$

with the Steklov-Poincare operator

$$\mathscr{S} : H^{\frac{1}{2}}(\partial\Omega) \to H^{-\frac{1}{2}}(\partial\Omega), \quad \text{with} \quad q \mapsto \partial_{\mathbf{n}}\omega,$$

where ω is the solution of the elliptic PDE

$$-\Delta\omega = 0, \quad \text{in } \Omega, \quad \omega = q, \quad \text{on } \partial\Omega.$$

Hence for each component controlled via a Dirichlet boundary condition we have to solve an additional PDE problem, which increases the computational costs drastically for fine spatial and temporal grids.

Other possibilities of implementing an $H^{\frac{1}{2}}$-norm or an $H^{\frac{1}{2}}$-semi-norm are based on the calculation of complicated boundary integrals, which can hardly be treated in the context of optimisation problems.

From the numerical point of view the most attractive choice of the control space is the $L^2(\partial\Omega)$. As mentioned before the theoretical justification for Dirichlet controls is now cumbersome. However, there is a conceptual access to the problem, which we want to briefly describe by means of the very simple PDE-constrained optimisation problem

$$\min_{u \in V, q \in \mathscr{Q}} J(u, q) = \frac{1}{2}\|u - \hat{u}\|_2^2 + \frac{\alpha}{2}\|q\|_2^2$$

subject to the time-independent Poisson problem

$$-\Delta u = f \quad \text{in } \Omega, \quad u = q \quad \text{on } \partial\Omega.$$

The idea is now to work with the very weak formulation of the state equation as constraint (see May et al. [27])

$$-(u, \Delta\varphi) + \langle q, \partial_n \varphi \rangle = (f, \varphi) \quad \forall \varphi \in H^2(\Omega) \cap H_0^1(\Omega),$$

and the spaces $V = L^2(\Omega)$ and $\mathscr{Q} = L^2(\partial\Omega)$. The so formulated problem admits a unique solution pair (u, q). Belgacem et al. [7] showed that μ-dependent solutions (u_μ, q_μ) of the optimisation problem

$$\min_{\substack{u_\mu \in H^1(\Omega), \\ q_\mu \in L^2(\partial\Omega)}} J(u_\mu, q_\mu)$$

subject to

$$\left(\nabla u_\mu, \nabla \varphi\right) + \frac{1}{\mu}\left\langle u_\mu - q_\mu, \varphi\right\rangle = (f, \varphi), \quad \forall \varphi \in H^1(\Omega)$$

with $\mu > 0$, converge to a solution (u, q) of the L^2-Dirichlet control problem with the very weak formulation of the Poisson problem as side condition as μ tends to zero.

Remark 2 It was shown by Hou et al. [23] that this concept of approximating Dirichlet controls by using the penalised Neumann conditions for small choices of μ works also for optimisation problems with the time-independent Navier-Stokes equations as PDE side condition and a certain choice of the cost functional.

However, for system (1) the presented theoretical background cannot easily be carried over due to the fact that a very weak solution of the time-dependent Navier-Stokes equations is only L^4-regular in space (see Farwig et al. [16]), which is neither sufficient for the presented cost functional nor for the existence theory of the convection-diffusion equation describing the evolution of the brightness function.

We are not limited to use Dirichlet controls. For us the choice of the boundary conditions is only a tool for the estimation of a reliable flow field which transports the brightness distribution in an appropriate manner. Thus, we can work with the above described Robin-type boundary conditions anyway. We state the optimisation problem after introducing appropriate vector spaces.

Definition 2 (Solenoidal Vector Spaces) We define the following vector spaces

$$H^1_{\mathrm{div}}(\Omega)^2 := \{\boldsymbol{\varphi} \in H^1(\Omega)^2 : \ \nabla \cdot \boldsymbol{\varphi} = 0 \text{ in a weak sense}\},$$
$$L^2_{\mathrm{div}}(\Omega)^2 \ = \overline{H^1_{\mathrm{div}}(\Omega)^2}^{\|\cdot\|_2}.$$

Definition 3 (Robin-Type Control for Image Interpolation) Find

$$\{\mathbf{u}, I\} \in L^2\left(0, T; H^1_{\mathrm{div}}(\Omega)^2\right) \times L^2\left(0, T; H^1(\Omega)\right)$$

and

$$\{\mathbf{q_u}, q_I\} \in L^2\left(0, T; L^2(\partial\Omega)^2\right) \times L^2\left(0, T; L^2(\partial\Omega)\right)$$

so that the functional

$$J(\{q_I, \mathbf{q_u}\}, I)$$

in Definition 1 is minimised, subject to the following weak formulation of the above mentioned coupled system of equations.

Definition 4 (Weak Formulation of the State Equation) For initial values $\mathbf{u}^0 \in L^2_{\text{div}}(\Omega)^2$ and $\mathscr{I}_1 \in L^2(\Omega)$ find a pair

$$\{\mathbf{u}, I\} \in L^2\left(0, T; H^1_{\text{div}}(\Omega)^2\right) \times L^2\left(0, T; H^1(\Omega)\right)$$

so that

$$\begin{aligned} \int_0^T \big(-(I, \partial_t \psi) + a_I(\mathbf{u}; I, \psi) + b_I(\mathbf{u}; q_I; I, \psi) \big) dt &= (\mathscr{I}_1, \psi(0)) \\ \int_0^T \big(-(\mathbf{u}, \partial_t \boldsymbol{\varphi}) + a_{\mathbf{u}}(\mathbf{u})(\boldsymbol{\varphi}) + b_{\mathbf{u}}(\mathbf{q}_{\mathbf{u}}; \mathbf{u})(\boldsymbol{\varphi}) \big) dt &= \left(\mathbf{u}^0, \boldsymbol{\varphi}(0)\right) \end{aligned} \tag{3}$$

is fulfilled for all test functions

$$\begin{aligned} \psi &\in \left\{ \psi \in L^2\left(0, T; H^1(\Omega)\right) \text{ and } \partial_t \psi \in L^2\left(0, T; \left(H^1(\Omega)\right)'\right) \right\}, \\ \boldsymbol{\varphi} &\in \left\{ \boldsymbol{\varphi} \in L^2\left(0, T; H^1_{\text{div}}(\Omega)^2\right) \text{ and } \partial_t \boldsymbol{\varphi} \in L^2\left(0, T; \left(H^1_{\text{div}}(\Omega)^2\right)'\right) \right\}. \end{aligned} \tag{4}$$

The bi- and semi-linear forms are defined as follows

$$\begin{aligned} a_I(\mathbf{u}; I, \psi) &:= \varepsilon (\nabla I, \nabla \psi) + (\mathbf{u} \cdot \nabla I, \psi), \\ a_{\mathbf{u}}(\mathbf{u})(\boldsymbol{\varphi}) &:= \nu (\nabla \mathbf{u}, \nabla \boldsymbol{\varphi}) + (\mathbf{u} \cdot \nabla \mathbf{u}, \boldsymbol{\varphi}), \\ b_I(\mathbf{u}; q_I; I, \psi) &:= \frac{1}{\mu_1} \langle I - q_I, \psi \rangle_{\partial\Omega} - \frac{1}{2} \langle (\mathbf{u} \cdot \mathbf{n}) I, \psi \rangle_{\partial\Omega}, \\ b_{\mathbf{u}}(\mathbf{q}_{\mathbf{u}}; \mathbf{u})(\boldsymbol{\varphi}) &:= \frac{1}{\mu_2} \langle \mathbf{u} - \mathbf{q}_{\mathbf{u}}, \boldsymbol{\varphi} \rangle_{\partial\Omega} - \frac{1}{2} \langle (\mathbf{u} \cdot \mathbf{n}) \mathbf{u}, \boldsymbol{\varphi} \rangle_{\partial\Omega} \end{aligned} \tag{5}$$

Remark 3 (Temporal Regularity) The above formulation has on first glance not enough regularity for a well-defined cost functional and meaningful initial conditions in I and $\mathbf{u}$. However, assume for a moment enough regularity to achieve the equivalent weak formulation

$$(\partial_t I, \tilde{\psi}) + a_I(\mathbf{u}; I, \tilde{\psi}) + b_I(\mathbf{u}; q_I; , \tilde{\psi}) = 0 \qquad \forall \tilde{\psi} \in H^1(\Omega)$$

after partial integration and using a test function $\psi(\mathbf{x}, t) = \bar{\psi}(t)\tilde{\boldsymbol{\psi}}(\mathbf{x})$. It is straightforward to show $\partial_t I \in L^2(0, T; H^1(\Omega)')$ for the assumed regularity of $I, \mathbf{u}$ and q_I in Definition 3 outgoing from the last equation. Thus, due to the Gelfand tripel

$$H^1(\Omega) \subset L^2(\Omega) \subset H^1(\Omega)'$$

we obtain $I \in C\left([0,T];L^2(\Omega)\right)$ by a standard result (cf. Evans [15]). The same thing can also be proven for the solenoidal spaces in the Navier-Stokes case (cf. Temam [39]).

Remark 4 (Strong Formulation of the Boundary Conditions) Under the assumption of sufficient regularity of the functions we can extract from the above stated weak formulations the following corresponding Robin boundary conditions:

$$\varepsilon \partial_n I = \frac{1}{\mu_1}(q_I - I) + \frac{1}{2}(\mathbf{u}\cdot\mathbf{n})\, I \qquad \text{on } \partial\Omega \times (0,T],$$

$$\nu \partial_{\mathbf{n}}\mathbf{u} - p\mathbf{n} = \frac{1}{\mu_2}(\mathbf{q_u} - \mathbf{u}) + \frac{1}{2}(\mathbf{u}\cdot\mathbf{n})\,\mathbf{u} \qquad \text{on } \partial\Omega \times (0,T].$$

In the next section we will prove the existence of minimisers of the optimisation problem in Definition 3.

4 Mathematical Theory of the Optimisation Problem

A first step towards a proof of the existence of minimisers of the optimisation problem in Definition 3 is to prove unique solvability of the weak formulation in Definition 4. Therefore, we consider at first the following result:

Theorem 1 *For $\mu_2 \in (0,1]$, $u^0 \in L^2(\Omega)^2$ and a fixed boundary function*

$$\mathbf{q_u} \in L^2\left(0,T;L^2(\partial\Omega)^2\right)$$

the Navier-Stokes system in the second equation of (3) has a unique solution

$$\mathbf{u} \in L^\infty\left(0,T;L^2_{div}(\Omega)^2\right) \cap L^2\left(0,T;H^1_{div}(\Omega)^2\right).$$

Proof We can obtain the result by a few simple modifications of the standard Galerkin technique as presented in Temam [39]. At first we obtain the a-priori bound

$$\int_0^T \left(\frac{d}{dt}\|\mathbf{u}(t)\|_2^2 + \nu\|\nabla\mathbf{u}(t)\|_2^2 + \frac{1}{\mu_2}\|\mathbf{u}(t)\|^2_{L^2(\partial\Omega)^2}\right) dt \le \frac{c}{\mu_2}\int_0^T \|\mathbf{q_u}(t)\|^2_{L^2(\Omega)^2}\, dt, \tag{6}$$

since

$$(\mathbf{u}\cdot\nabla\mathbf{u},\mathbf{u}) = \frac{1}{2}\int_{\partial\Omega}(\mathbf{u}\cdot\mathbf{n})\mathbf{u}^2 ds, \tag{7}$$

in contrast to the usual proof. With inequality (6) we obtain the usual (weak and strong) convergence properties of a certain subsequence.

The properties are then used to prove the convergence of the sequence of approximative solutions $\mathbf{u}^m$ of the Navier-Stokes system. The only difference to the standard proof is the convergence of the semi-linear boundary form

$$\int_0^T \int_{\partial\Omega} ((\mathbf{u}^m \cdot \mathbf{n})\mathbf{u}^m - (\mathbf{u} \cdot \mathbf{n})\mathbf{u})\, \boldsymbol{\varphi} ds dt \to 0.$$

Therefore, we set $\mathbf{w}^m = \mathbf{u}^m - \mathbf{u}$ and consider

$$\begin{aligned} \left| \int_0^T \int_{\partial\Omega} ((\mathbf{w}^m \cdot \mathbf{n})\, \mathbf{u}^m + (\mathbf{u} \cdot \mathbf{n})\, \mathbf{w}^m)\, \boldsymbol{\varphi} ds dt \right| &\leq \left| \int_0^T \langle (\mathbf{w}^m \cdot \mathbf{n})\, \mathbf{u}^m, \boldsymbol{\varphi} \rangle_{\partial\Omega}\, dt \right| \\ &+ \left| \int_0^T \int_{\partial\Omega} (\mathbf{u} \cdot \mathbf{n})\, \mathbf{w}^m \boldsymbol{\varphi} ds dt \right|. \end{aligned} \tag{8}$$

As test functions $\boldsymbol{\varphi}$ we choose functions from a subset, which is sufficiently smooth on the whole boundary and the time interval. The first term of the right hand side in (8) is transformed in domain integrals by

$$\int_0^T \langle (\mathbf{w}^m \cdot \mathbf{n})\, \mathbf{u}^m, \boldsymbol{\varphi} \rangle_{\partial\Omega}\ dt = \int_0^T (\mathbf{w}^m \cdot \nabla \mathbf{u}^m, \boldsymbol{\varphi})\ dt + \int_0^T (\mathbf{w}^m \cdot \nabla \boldsymbol{\varphi}, \mathbf{u}^m)\ dt,$$

since $\mathbf{u}^m$ and $\mathbf{w}^m$ are solenoidal. Due to the smoothness of the test function it is easy to obtain that the terms on the right hand side vanish in the limit, since $\mathbf{u}^m$ converges strongly in $L^2(0, T; L^2(\Omega)^2)$. The second term of the right hand side in (8) can be estimated

$$\left| \int_0^T \int_{\partial\Omega} (\mathbf{u} \cdot \mathbf{n})\, \mathbf{w}^m \boldsymbol{\varphi}\ ds dt \right| \leq \sup_{(\mathbf{x},t) \in \partial\Omega \times [0,T]} |\boldsymbol{\varphi}(\mathbf{x}, t)| \int_0^T |\, \langle \mathbf{u}, \mathbf{w}^m \rangle_{\partial\Omega}\, |\, dt$$

Weak convergence in $L^2(0, T; L^2(\partial\Omega)^2)$ yields that this term is also vanishing. Thus, the whole convergence of the Galerkin approximations in the weak formulation can be obtained by standard continuity arguments.

For the uniqueness we assume the existence of two different solutions for the same initial and boundary data. The difference is given by $\mathbf{w}^m = \mathbf{u} - \mathbf{v}$ and we find the identity

$$\frac{1}{2}\frac{d}{dt}\|\mathbf{w}^m\|_2^2 + \nu\|\nabla \mathbf{w}^m\|_2^2 + \frac{1}{\mu_2}\|\mathbf{w}^m\|_{L^2(\partial\Omega)^2}^2 = -\frac{1}{2}\left((\mathbf{w}^m \cdot \nabla \mathbf{u}, \mathbf{w}^m) - (\mathbf{w}^m \cdot \nabla \mathbf{w}^m, \mathbf{u})\right),$$

after standard manipulations and by using Eq. (7). The Ladyzhenskaya inequality in two space dimensions

$$\|\mathbf{w}^m\|_{L^4(\Omega)^2} \leq c\|\mathbf{w}^m\|_2^{\frac{1}{2}} \|\nabla \mathbf{w}^m\|_2^{\frac{1}{2}}$$

is used in combination with Young's inequality to find

$$\frac{d}{dt}\|\mathbf{w}^m(t)\|_2^2 \leq \beta(t)\|\|\mathbf{w}^m(t)\|_2^2.$$

with

$$\beta(t) := c(\nu, \Omega)\left(\|\mathbf{u}(t)\|_{H^1(\Omega)^2}^2 + \|\mathbf{u}(t)\|_2^2\|\mathbf{u}(t)\|_{H^1(\Omega)^2}^2\right)$$

Gronwall's inequality and $\mathbf{w}^m(0,\mathbf{x}) = 0$ yields the uniqueness, since

$$\int_0^t \beta(s)\, ds \leq c(\nu,\Omega)\left(\int_0^t \|\mathbf{u}(s)\|_{H^1(\Omega)^2}^2\, ds + \operatorname*{ess\,sup}_{s\in[0,t]}\|\mathbf{u}(s)\|_2^2 \int_0^t \|\mathbf{u}(s)\|_{H^1(\Omega)^2}^2\, ds\right)$$

stays bounded due to $\mathbf{u} \in L^\infty\left(0,T;L^2_{\text{div}}(\Omega)^2\right) \cap L^2\left(0,T;H^1_{\text{div}}(\Omega)^2\right)$, which was obtained by the a-priori bound in formula (6). □

Theorem 2 *For fixed parameters μ_1 and μ_2 in $(0,1]$ and boundary functions $q_I \in L^2\left(0,T;L^2(\partial\Omega)\right)$ and $\mathbf{q_u} \in L^2\left(0,T;L^2(\partial\Omega)^2\right)$ there exists a unique solution pair*

$$\{I_\mu, \mathbf{u}_\mu\} \in L^2(0,T;H^1(\Omega)) \times L^2(0,T;H^1_{div}(\Omega)^2).$$

Proof We consider the two aspects existence and uniqueness. We skip the index μ_i with $i = 1,2$ for abbreviation:

(Existence)

We use the standard Galerkin technique. Since the convection-diffusion equation for the brightness I is not coupling back to the Navier-Stokes system we can argue in the following way. By Theorem 1 we have the existence of a unique transport field

$$\mathbf{u} \in L^\infty\left(0,T;L^2_{\text{div}}(\Omega)^2\right) \cap L^2\left(0,T;H^1_{\text{div}}(\Omega)^2\right).$$

Hence, we find in the standard way the a-priori bound

$$\int_0^T \left(\frac{d}{dt}\|I(t)\|_2^2 + \varepsilon\|\nabla I(t)\|_2^2 + \frac{1}{\mu_1}\|I(t)\|_{L^2(\partial\Omega)}^2\right) dt \leq \frac{c}{\mu_1}\int_0^T \|q_I(t)\|_{L^2(\partial\Omega)}^2\, dt, \tag{9}$$

since

$$(\mathbf{u}\cdot\nabla I, I) - \frac{1}{2}\langle(\mathbf{u}\cdot\mathbf{n})I, I\rangle_{\partial\Omega} = 0, \tag{10}$$

for the transport field $\mathbf{u}$. By the standard Galerkin technique and modifications mentioned in the proof of Theorem 1 we find easily the existence of the solution $I \in L^2\left(0,T;H^1(\Omega)\right)$.

(Uniqueness)

The uniqueness of a solution pair $\{I,\mathbf{u}\}$ can be achieved by assuming as usual the existence of two solution pairs $\{I_1,\mathbf{u}_1\}$ and $\{I_2,\mathbf{u}_2\}$ for the same data and building the difference for the systems. We use the notation $K = I_1 - I_2$ and $\mathbf{w}^m = \mathbf{u}_1 - \mathbf{u}_2$. Due to the independence of the Navier-Stokes part of the system from K and the uniqueness of the Navier Stokes solution we have $\mathbf{u}_1 = \mathbf{u}_2$. Thus, the convection-diffusion part is a linear equation, since we can use Eq. (10) for $I = K$. The rest of the argumentation is standard and yields $K = 0$ by Gronwall's lemma. □

Now we are able to prove the existence of a minimiser of the optimisation problem in Definition 3.

Theorem 3 (Solution of the Optimisation Problem) *For $\mu := \mu_1 = \mu_2 \in (0,1]$ fixed we have the existence of at least one minimiser*

$$I_\mu \in L^2\left(0,T;H^1(\Omega)\right)$$
$$\mathbf{u}_\mu \in L^2\left(0,T;H^1_{div}(\Omega)^2\right)$$
$$q_{I,\mu} \in L^2\left(0,T;L^2(\partial\Omega)\right)$$
$$\mathbf{q}_{\mathbf{u},\mu} \in L^2\left(0,T;L^2(\partial\Omega)^2\right)$$

of the optimisation problem in Definition 3.

Proof Thanks to the previous theorem we have the existence of solutions of the state equation and therefore the admissible set is not empty.

We skip the index μ for abbreviation, collect the controls in the overall vector $\mathbf{q} := (q_I, \mathbf{q}_\mathbf{u}) \in L^2(\partial\Omega)^3$ and choose then a minimising sequence $\{I^{(k)}, \mathbf{u}^{(k)}, \mathbf{q}^{(k)}\}$ in this set with the property

$$\lim_{k\to\infty} J(\mathbf{q}^{(k)}, I^{(k)}) = \inf_{\{I,\mathbf{q}\}} J(\mathbf{q}, I) =: \theta.$$

By using Young's inequality we obtain a uniform bound for $\mathbf{q}$:

$$\|\mathbf{q}^{(k)}\|_{L^2\left(0,T;L^2(\partial\Omega)^3\right)} \leq \frac{1}{\alpha} J(\mathbf{q}^{(k)}, I^{(k)}) + \frac{1}{2} \leq B.$$

Thus, the controls q_I and $\mathbf{q}_\mathbf{u}$ are bounded in $L^2\left(0,T;L^2(\partial\Omega)\right)$ and $L^2\left(0,T;L^2(\partial\Omega)^2\right)$. Hence, by the energy estimates (6) and (9) we receive all necessary uniform bounds for $I^{(k)}$ and $\mathbf{u}^{(k)}$. Finally we find

$$I^{(k)} \in L^\infty(0,T;L^2(\Omega)) \cap L^2(0,T;H^1(\Omega)) \cap L^2(0,T;L^2(\partial\Omega)) \tag{11}$$
$$\mathbf{u}^{(k)} \in L^\infty(0,T;L^2(\Omega)^2) \cap L^2(0,T;H^1_{\text{div}}(\Omega)^2) \cap L^2(0,T;L^2(\partial\Omega)^2) \tag{12}$$

We can then extract the subsequences

$$I^{(k')} \rightharpoonup I \quad \begin{array}{ll} \text{weakly} & \text{in } L^2(0,T;H^1(\Omega)), \\ \text{weakly-}\star & \text{in } L^\infty(0,T;L^2(\Omega)), \\ \text{weakly} & \text{in } L^2(0,T;L^2(\partial\Omega)), \end{array} \quad \text{as } k' \to \infty,$$

and

$$\mathbf{u}^{(k')} \rightharpoonup \mathbf{u} \quad \begin{array}{ll} \text{weakly} & \text{in } L^2(0,T;H^1_{\mathrm{div}}(\Omega)^2), \\ \text{weakly-}\star & \text{in } L^\infty(0,T;L^2(\Omega)^2), \\ \text{weakly} & \text{in } L^2(0,T;L^2(\partial\Omega)^2), \end{array} \quad \text{as } k' \to \infty,$$

By compactness results we obtain also the strong convergence properties

$$I^{(k')} \to I \quad \text{in } L^2(0,T;L^2(\Omega)), \quad \mathbf{u}^{(k')} \to \mathbf{u} \quad \text{in } L^2(0,T;L^2(\Omega)^2),$$

of the subsequences. Thus, passing to the limit in the state equation is a standard task.

It remains to show that the pair $\{I, \mathbf{u}, \mathbf{q}\}$ is in fact a minimum of $J(\cdot,\cdot)$. We use the obtained convergence properties to compute

$$\begin{aligned} \theta &= \lim_{k\to\infty} J(I^{(k)}, \mathbf{q}^{(k)}) = \lim_{k\to\infty} \left(\frac{1}{2} \sum_{j=1}^{N} \|I^{(k)}(t_j) - \mathscr{I}_j\|_2^2 + \frac{\alpha}{2} \int_0^T \|\mathbf{q}^{(k)}(t)\|^2_{L^2(\partial\Omega)^3}\, dt \right) \\ &= \frac{1}{2} \sum_{j=1}^{N} \|I(t_j) - \mathscr{I}_j\|_2^2 + \liminf_{k\to\infty} \frac{\alpha}{2} \int_0^T \|\mathbf{q}(t)\|^2_{L^2(\partial\Omega)^3}\, dt. \end{aligned}$$

Due to the continuity and convexity of the norm $\|\cdot\|_{L^2(0,T;L^2(\partial\Omega)^3)}$ the norm is also weakly lower semicontinuous. Thus, we find

$$\theta \geq \frac{1}{2} \sum_{j=1}^{N} \|I(t_j) - \mathscr{I}_j\|_2^2 + \frac{\alpha}{2} \int_0^T \|\mathbf{q}(t)\|^2_{L^2(\partial\Omega)^3}\, dt = J(I, \mathbf{q}),$$

which proves the optimality of the pair $\{I, \mathbf{u}, \mathbf{q}\}$. □

5 Numerical Solution Process and Further Specifics

5.1 Optimisation Algorithm

We briefly present the optimisation algorithm. All following aspects are very well summarised in the thesis of Meidner [28]. By Theorem 1 we know that the state equation of our PDE constrained optimisation problem is uniquely solvable. Hence we can introduce the solution operator and find $\{\mathbf{u}, I\} = S(\mathbf{q}_\mathbf{u}, q_I)$. By means of this operator we can transform the original problem into an unconstrained problem

$$j(\tilde{\mathbf{q}}) = J(S(\tilde{\mathbf{q}}), \tilde{\mathbf{q}}), \qquad \text{with } \tilde{\mathbf{q}} = \{\mathbf{q}_\mathbf{u}, q_I\}.$$

The first-order necessary condition is then given by

$$j'(\mathbf{q})(\delta\mathbf{q}) = 0 \qquad \forall \delta\mathbf{q} \in \mathcal{Q},$$

where $\mathcal{Q}$ denotes the vector space for the controls.

We use now a Newton-type algorithm to find a solution of the last equation. Therefore we represent the first and second variationals derivative of $j(\cdot)$ by auxiliary variables, which have to be evaluated by solving additional PDE problems. The key for this representation is the identity

$$j(\mathbf{q}) = J(\mathbf{q}, \mathbf{u}) = \mathcal{L}(\mathbf{q}, \mathbf{u}, \mathbf{z}), \tag{13}$$

where $\mathcal{L}(\cdot)$ denotes the Lagrangian.

The first derivative can be expressed by

$$j'(\mathbf{q})(\delta\mathbf{q}) = \mathcal{L}'_\mathbf{q}(\mathbf{q}, \mathbf{u}, \mathbf{z})(\delta\mathbf{q}) \qquad \forall \delta\mathbf{q} \in \mathcal{Q}.$$

Therefore we have to compute u and z by solving the primal and the adjoint equations

$$\mathcal{L}'_\mathbf{z}(\mathbf{q}, \mathbf{u}, \mathbf{z})(\varphi) = 0 \qquad \forall \varphi \in V \qquad \text{(Primal Eq.)},$$
$$\mathcal{L}'_\mathbf{u}(\mathbf{q}, \mathbf{u}, \mathbf{z})(\varphi) = 0 \qquad \forall \varphi \in V \qquad \text{(Adjoint Eq.)}.$$

The second derivative is given by

$$j''(\mathbf{q})(\delta\mathbf{q}, \tau\mathbf{q}) = \mathcal{L}''_{\mathbf{qq}}(\mathbf{q}, \mathbf{u}, \mathbf{z})(\delta\mathbf{q}, \tau\mathbf{q}) + \mathcal{L}''_{\mathbf{uq}}(\mathbf{q}, \mathbf{u}, \mathbf{z})(\delta\mathbf{u}, \tau\mathbf{q}) + \mathcal{L}''_{\mathbf{zq}}(\mathbf{q}, \mathbf{u}, \mathbf{z})(\delta\mathbf{z}, \tau\mathbf{q}).$$

Beside the primal and the adjoint solutions u and z we need now two further variables δu and δz, which can be obtained by solving the following equations

$$\begin{aligned} \mathscr{L}''_{\mathbf{qz}}(\mathbf{q},\mathbf{u},\mathbf{z})(\boldsymbol{\delta}\mathbf{q},\boldsymbol{\varphi}) + \mathscr{L}''_{\mathbf{uz}}(\mathbf{q},\mathbf{u},\mathbf{z})(\boldsymbol{\delta}\mathbf{u},\boldsymbol{\varphi}) &= 0 \qquad \text{(Tangent Eq.)} \\ \mathscr{L}''_{\mathbf{qu}}(\mathbf{q},\mathbf{u},\mathbf{z})(\boldsymbol{\delta}\mathbf{q},\boldsymbol{\varphi}) + \mathscr{L}''_{\mathbf{uu}}(\mathbf{q},\mathbf{u},\mathbf{z})(\boldsymbol{\delta}\mathbf{u},\boldsymbol{\varphi}) & \\ + \mathscr{L}''_{\mathbf{zu}}(\mathbf{q},\mathbf{u},\mathbf{z})(\boldsymbol{\delta}\mathbf{z},\boldsymbol{\varphi}) &= 0 \qquad \text{(Additional Adjoint Eq.)} \end{aligned}$$

Algorithm 1 summarise theses principles.

Algorithm 1 Newton-CG Algorithm

1: Choose an initial $q^0 \in \mathscr{Q}_h$, $\mu_0 \in R \cup \{+\infty\}$ and set $k = 0$.
2: Solve the State Eq. : $\mathscr{L}'_z(q,u,z)(\varphi) = 0 \qquad \forall \varphi \in V$
3: Evaluate the cost functional $J(q,u)$
4: Solve the Dual Eq.: $\mathscr{L}'_u(q,u,z)(\varphi) = 0 \qquad \forall \varphi \in V$
5: Evaluate the residual : $f := -j'(q^k)(\delta q^k)$
6: If $\|f\| <$ TOL then STOP
7: Solve the system

$$j''(q^{(k)})(\delta q_i^{(k)}, \tau q_j^{(k)}) = -j'(q^{(k)})(\tau q_j^{(k)}) \tag{14}$$

with a CG-method. For each iteration of the CG method we perform

7.1: Solve the Tangent Eq.: $\mathscr{L}''_{qz}(q,u,z)(\delta q,\varphi) + \mathscr{L}''_{uz}(q,u,z)(\delta u,\varphi) = 0$.
7.2: Solve the Additional Adjoint Eq.:

$$\begin{aligned} \mathscr{L}''_{qu}(q,u,z)(\delta q,\varphi) + \mathscr{L}''_{uu}(q,u,z)(\delta u,\varphi) & \\ + \mathscr{L}''_{zu}(q,u,z)(\delta z,\varphi) &= 0 \end{aligned}$$

7.3: STOP the CG-method if the residual of the linear system drops below a given tolerance.

8: Update the control

$$q^{(k+1)} = q^{(k)} + \lambda_k q^{(k)},$$

The relaxation parameter λ_k is used to globalise the Newton method.
9: Go back to Step 2.

Remark 5 (Application of the CG Method in the Algorithm) The CG-method allows a matrix-free solution process, which means that we do not have to assemble the Hessian matrix, which saves computational effort. The desired number of iterations to solve the system (14) for a given tolerance depends on the condition of the Hessian matrix. In the case of ill-posed problems the condition number increases, when the regularisation parameter decreases. The convergence behaviour of the CG-method is then very bad. Usually we stop the iteration after a certain amount of steps, unless the threshold for the residuum was reached. Then we work with a so called inexact Newton method.

5.2 PDE Subproblems

The PDE subproblems mentioned in Algorithm 1 are solved by a Rothe method, which means that the problems are first discretised in the time variable and then in the space variable. We will start with the time discretisation.

5.2.1 Time Discretisation

In the used Software library RoDoBo [6] we have the possibility to use either a discontinuous Galerkin $dG(r)$ method or a continuous Galerkin $cG(r)$ method for the time discretisation. The use of Galerkin discretisation was preferred by the authors of the library, since it is necessary to preserve the property that 'discretise-then-optimise' and 'optimise-then-discretise' commute.

The $cG(r)$ method consists of continuous trial functions of degree r and discontinuous test functions of degree $r-1$, while the $dG(r)$ method is based on the use of discontinuous trial and test functions of degree r. Using a $dG(0)$ method, where all occurring integrals are evaluated with the box rule, leads directly to the standard backward Euler scheme. The $cG(1)$ method, where all occurring temporal integrals are approximated with the trapezoidal rule, generates the Crank-Nicolson scheme. For the following calculations we use these two methods only.

For the spatial discretisation of the resulting quasi-stationary equations we use the well-known finite element method.

5.2.2 Spatial Discretisation

To describe the conceptual features of our finite element approach, we consider the following abstract weak formulation for the quasi-stationary equation:

For a given q, find a suitable $u \in V$ such that

$$a(u,\varphi) + b(q;u,\varphi) = l(\varphi) \quad \forall \varphi \in V \tag{15}$$

with the bilinear forms $a(u,\varphi), b(q;u,\varphi)$ and the linear form $l(\varphi)$.

By choosing a conforming ansatz space V_h we derive the following Galerkin equations:

$$a(u_h,\varphi_h) + b(q;u_h,\varphi_h) = l(\varphi_h) \qquad \forall \varphi_h \in V_h. \tag{16}$$

Due to an appropriate choice of the space V_h and the linearity of the forms we end up with the following system of equations

$$A_h x_h = b_h, \qquad \text{with } u_h = \sum_{i=1}^{N} x_{h,i} e^{(i)},$$

which is then solved by a multigrid method.

For all our calculations we used the ansatz space V_h containing continuous functions, which are piecewise bilinear polynomials on a decomposition of the computational domain into regular quadrilaterals:

$$\hat{V}_h := \{u_h : \bar{\Omega} \to \mathbb{R} \mid u_h \in C(\bar{\Omega}),\ u_h|_T \in Q_1\} \tag{17}$$

For a detailed description of this methodology see the monographs of Braess [9] and Brenner et al. [10].

Remark 6 (Nonlinear PDEs) In the case of nonlinear PDEs, e.g. the Navier-Stokes system, we have to linearise the equation. In this case we use also a Newton method and solve then in each step of the Newton method a PDE which fits in the above presented setting.

5.3 Comments on Boundary Conditions

Since we consider boundary identification problems a special focus of this work is on the treatment of boundary conditions. The suggested penalised Neumann approach depends on the choice of the parameter μ. Decreasing the parameter μ the condition of the discrete system is getting worse. A way out of this dilemma was presented by Juntunen et al. [24] for the Poisson problem. This concept can easily be carried over to convection-diffusion equations and the Navier-Stokes system.

5.3.1 Convection-Diffusion Equation

We consider the following convection-diffusion-reaction equation

$$\begin{aligned} -\nu\Delta u + \beta\cdot\nabla u + cu &= f && \text{in } \Omega, \\ \nu\partial_n u &= \frac{1}{\mu}(q_D - u) + \frac{1}{2}(\boldsymbol{\beta}\cdot\mathbf{n})\,u && \text{on } \partial\Omega. \end{aligned} \tag{18}$$

We use the bilinear forms

$$a(u,\varphi) := \nu\,(\nabla u, \nabla\varphi) + (\beta\cdot\nabla u, \varphi) + (cu, \varphi)$$

for the domain and

$$\begin{aligned} b(q_D; u, \varphi) := &-\frac{\nu\delta}{\mu+\delta}\left(\langle \partial_{\mathbf{n}} u, \varphi\rangle_{\partial\Omega} + \langle u - q_D, \partial_{\mathbf{n}}\varphi\rangle_{\partial\Omega}\right) + \frac{1}{\mu+\delta}\langle u - q_D, \varphi\rangle_{\partial\Omega} \\ &- \frac{\nu\mu\delta}{\mu+\delta}\langle \partial_{\mathbf{n}} u, \partial_{\mathbf{n}}\varphi\rangle_{\partial\Omega} - \frac{\mu}{2(\mu+\delta)}\langle(\boldsymbol{\beta}\cdot\mathbf{n})u, \varphi\rangle_{\partial\Omega} \\ &+ \frac{\mu\delta}{2(\mu+\delta)}\langle(\boldsymbol{\beta}\cdot\mathbf{n})u, \partial_{\mathbf{n}}\varphi\rangle_{\partial\Omega}\,, \end{aligned} \tag{19}$$

for the boundary to formulate the problem weakly

$$a(u,\varphi) + b(q_D; u, \varphi) = (f, \varphi) \quad \forall \varphi \in V. \tag{20}$$

Lemma 1 *A solution of problem (18) also satisfies Eq. (20).*

Proof We integrate the first equation in (18) over the domain after multiplying with an arbitrary test function $\varphi \in V$. Integration by parts yields

$$a(u,\varphi) - \nu\langle \partial_{\mathbf{n}} u, \varphi\rangle_{\partial\Omega} = (f, \varphi)\,. \tag{21}$$

We multiply now the boundary part of Eq. (18) with the same test function and integrate over the boundary. Then we multiply both sides by $\frac{\mu}{\mu+\delta}$ and obtain

$$\frac{\mu\nu}{\mu+\delta}\langle \partial_{\mathbf{n}} u, \varphi\rangle_{\partial\Omega} = \frac{1}{\mu+\delta}\langle q_D - u, \varphi\rangle_{\partial\Omega} + \frac{\mu}{2(\mu+\delta)}\langle(\boldsymbol{\beta}\cdot\mathbf{n})u, \varphi\rangle_{\partial\Omega} \tag{22}$$

Doing the same again with the test function $\partial_{\mathbf{n}}\varphi$ and the factor $-\frac{\delta\mu}{\mu+\delta}$ we get

$$\begin{aligned} -\frac{\nu\mu\delta}{\mu+\delta}\langle \partial_{\mathbf{n}} u, \partial_{\mathbf{n}}\varphi\rangle_{\partial\Omega} = &-\frac{\delta}{\mu+\delta}\langle q_D - u, \partial_{\mathbf{n}}\varphi\rangle_{\partial\Omega} \\ &- \frac{\mu\delta}{2(\mu+\delta)}\langle(\boldsymbol{\beta}\cdot\mathbf{n})u, \partial_{\mathbf{n}}\varphi\rangle_{\partial\Omega} \end{aligned} \tag{23}$$

Equation (20) is now the sum of Eqs. (21)–(23). □

The bilinear form $b(q_D; u, \varphi)$ can even be evaluated for the case $\mu = 0$. We obtain then a Nitsche type formulation (Nitsche [30]) for the convection-diffusion equation

$$b_{\mathrm{Ni}}(q_D; u, \varphi) = -\nu\left(\langle \partial_{\mathbf{n}} u, \varphi\rangle_{\partial\Omega} + \langle u - q_D, \partial_{\mathbf{n}}\varphi\rangle_{\partial\Omega}\right) + \frac{1}{\delta}\langle u - q_D, \varphi\rangle_{\partial\Omega}\,. \tag{24}$$

Remark 7 (Linear Transport Equation) In the case of pure transport, $\nu = 0$, the boundary form $b(q_D; u, \varphi)$ reads

$$b(q_D; u, \varphi) = \frac{1}{\mu + \delta} \left(\langle u - q_D, \varphi \rangle_{\partial\Omega} - \frac{\mu}{2} \langle (\boldsymbol{\beta} \cdot \mathbf{n})\, u, \varphi \rangle_{\partial\Omega} + \frac{\delta\mu}{2} \langle (\boldsymbol{\beta} \cdot \mathbf{n})\, u, \partial_{\mathbf{n}} \varphi \rangle_{\partial\Omega} \right)$$

For an appropriate choice $\delta \geq \delta_0 > 0$ we obtain by setting $\mu = 0$ a Nitsche-type term for the realisation of Dirichlet boundary data for the pure transport equation

$$b(q_D; u, \varphi) = \frac{1}{\delta} \langle u - q_D, \varphi \rangle_{\partial\Omega} .$$

We are able to set Dirichlet conditions only on the inflow boundary Γ_{In}, that means all $\mathbf{x} \in \partial\Omega$ with $\boldsymbol{\beta} \cdot \mathbf{n} < 0$, in the following way

$$0 < \delta := -\frac{1}{(\boldsymbol{\beta} \cdot \mathbf{n})},$$

we obtain

$$b(q_D; u, \varphi) := -\langle (\boldsymbol{\beta} \cdot \mathbf{n})(u - q_D), \varphi \rangle_{\Gamma_{In}} . \tag{25}$$

This is consistent with a suggestion for Nitsche-type inflow presented in the work of Freund et al. [17].

5.3.2 Navier-Stokes System

For $V = H_0^1(\Omega)^n$ the Navier-Stokes system

$$\begin{aligned} -\nu \Delta \mathbf{u} + \mathbf{u} \cdot \nabla \mathbf{u} + \nabla p &= f \qquad \text{in } \Omega \\ \nabla \cdot \mathbf{u} &= 0 \qquad \text{in } \Omega \end{aligned} \tag{26}$$

can be weakly stated by

$$\begin{aligned} \nu\, (\nabla \mathbf{u}, \nabla \boldsymbol{\varphi}) + (\mathbf{u} \cdot \nabla \mathbf{u}, \boldsymbol{\varphi}) - (p, \nabla \cdot \boldsymbol{\varphi}) &= (\mathbf{f}, \boldsymbol{\varphi}) \qquad \forall \boldsymbol{\varphi} \in V \\ (\nabla \cdot \mathbf{u}, \psi) &= 0 \qquad \forall \psi \in M \end{aligned} \tag{27}$$

with $M = L^2(\Omega)$. In the case $V = H^1(\Omega)^n$ the additional boundary bilinear form

$$b(\{\mathbf{u}, p\}, \boldsymbol{\varphi}) := -\nu \langle \partial_{\mathbf{n}} \mathbf{u}, \boldsymbol{\varphi} \rangle_{\partial\Omega} + \langle p\mathbf{n}, \boldsymbol{\varphi} \rangle_{\partial\Omega} , \tag{28}$$

occurs in the above weak formulation. For the following strongly formulated Robin-type boundary conditions

$$\nu \partial_{\mathbf{n}} \mathbf{u} - p\mathbf{n} = \frac{1}{\mu} (\mathbf{q}_D - \mathbf{u}) + \frac{1}{2} (\mathbf{u} \cdot \mathbf{n}) \mathbf{u} \tag{29}$$

we obtain a well posed problem formulation with the boundary semi-linear form

$$b(\mathbf{q}_D; \mathbf{u})(\boldsymbol{\varphi}) := \frac{1}{\mu} \langle (\mathbf{u} - \mathbf{q}_D), \boldsymbol{\varphi} \rangle_{\partial\Omega} - \frac{1}{2} \langle (\mathbf{u} \cdot \mathbf{n}) \mathbf{u}, \boldsymbol{\varphi} \rangle_{\partial\Omega} . \tag{30}$$

Remark 8 (Nonlinear Term and Solvability Theory) Since

$$(\mathbf{u} \cdot \nabla \mathbf{u}, \mathbf{u}) = \frac{1}{2} \langle (\mathbf{u} \cdot \mathbf{n}) \mathbf{u}, \mathbf{u} \rangle_{\partial\Omega}$$

we find similar uniform bounds for the Galerkin technique, which is used in the solvability theory. This justifies the specific form of $b(\mathbf{q}_D; \{\mathbf{u}, p\})(\boldsymbol{\varphi})$.

Analogously to the convection-diffusion-reaction equation we can formulate a stabilised semi-linear form by

$$\begin{aligned} b_\mu^\delta(\mathbf{q}_D; \{\mathbf{u}, p\})(\boldsymbol{\varphi}) := & -\frac{\delta}{\mu + \delta} \left(\langle \nu \partial_{\mathbf{n}} \mathbf{u} - p\mathbf{n}, \boldsymbol{\varphi} \rangle_{\partial\Omega} + \langle \mathbf{u} - \mathbf{q}_D, \nu \partial_{\mathbf{n}} \boldsymbol{\varphi} + \psi \mathbf{n} \rangle_{\partial\Omega} \right) \\ & + \frac{1}{\mu + \delta} \langle \mathbf{u} - \mathbf{q}_D, \boldsymbol{\varphi} \rangle_{\partial\Omega} - \frac{\mu}{2(\mu + \delta)} \langle (\mathbf{u} \cdot \mathbf{n}) \mathbf{u}, \boldsymbol{\varphi} \rangle_{\partial\Omega} \\ & - \frac{\mu\delta}{\delta + \mu} \langle \nu \partial_{\mathbf{n}} \mathbf{u} - p\mathbf{n}, \nu \partial_{\mathbf{n}} \boldsymbol{\varphi} + \psi \mathbf{n} \rangle_{\partial\Omega} \\ & + \frac{\mu\delta}{2(\delta + \mu)} \langle (\mathbf{u} \cdot \mathbf{n}) \mathbf{u}, \nu \boldsymbol{\varphi} + \psi \mathbf{n} \rangle_{\partial\Omega} \end{aligned} \tag{31}$$

While $b_\mu^0(\cdot;\cdot)(\cdot)$ corresponds to the penalty formulation the parameter choice $\mu = 0$ and $\delta = \gamma(h)$ results in a Nitsche-type formulation for the Navier-Stokes system

$$\begin{aligned} b_0^{\gamma(h)}(\mathbf{q}_D; \{\mathbf{u}, p\})(\boldsymbol{\varphi}) := & - \langle \partial_{\mathbf{n}} \mathbf{u} - p\mathbf{n}, \boldsymbol{\varphi} \rangle_{\partial\Omega} - \langle \mathbf{u} - \mathbf{q}_D, \partial_{\mathbf{n}} \boldsymbol{\varphi} + \psi \mathbf{n} \rangle_{\partial\Omega} \\ & + \frac{1}{\gamma(h)} \langle \mathbf{u} - \mathbf{q}_D, \boldsymbol{\varphi} \rangle_{\partial\Omega} . \end{aligned} \tag{32}$$

This form is almost the same as the one proposed in Becker [3].

Lemma 2 *A strong solution pair $\{\mathbf{u}, p\}$ of the Navier Stokes system (26) with the boundary condition (29) satisfies also the equation*

$$\begin{aligned} \nu\,(\nabla\mathbf{u}, \nabla\boldsymbol{\varphi}) + (\mathbf{u}\cdot\nabla\mathbf{u}, \boldsymbol{\varphi}) + b_\mu^\delta(\mathbf{q}_D; \{\mathbf{u}, p\})(\boldsymbol{\varphi}) - (p, \nabla\cdot\boldsymbol{\varphi}) &= (\mathbf{f}, \boldsymbol{\varphi}) \qquad \forall \boldsymbol{\varphi} \in V, \\ (\nabla\cdot\mathbf{u}, \psi) &= 0 \qquad \forall \psi \in M. \end{aligned} \tag{33}$$

Proof By multiplying the classical Navier-Stokes equations with arbitrary test functions $\boldsymbol{\varphi} \in V$ and $\psi \in M$, integrating over the domain Ω and partial integration we obtain Eq. (27) with an additional semi-linear form $b(\mathbf{q}_D; \{\mathbf{u}, p\})(\boldsymbol{\varphi})$ like in Eq. (30).

By multiplying the boundary condition (29) with $\boldsymbol{\varphi}$ and integration over the boundary we obtain after multiplying with $\frac{\mu}{\mu+\delta}$

$$\begin{aligned} \frac{\mu}{\mu+\delta}\,\langle \nu\partial_{\mathbf{n}}\mathbf{u} - p\mathbf{n}, \boldsymbol{\varphi}\rangle_{\partial\Omega} + \frac{1}{\mu+\delta}\,\langle \mathbf{u} - \mathbf{q}_D, \boldsymbol{\varphi}\rangle_{\partial\Omega} \\ - \frac{\mu}{2(\mu+\delta)}\,\langle (\mathbf{u}\cdot\mathbf{n})\mathbf{u}, \boldsymbol{\varphi}\rangle_{\partial\Omega} = 0 \end{aligned} \tag{34}$$

Furthermore we multiply the boundary condition with the test function

$$\nu\partial_{\mathbf{n}}\boldsymbol{\varphi} + \psi\mathbf{n},$$

and integrate again over the boundary. Afterwards we multiply with the factor $-\frac{\mu\delta}{\mu+\delta}$ and obtain

$$\begin{aligned} -\frac{\mu\delta}{\mu+\delta}\,\langle \nu\partial_{\mathbf{n}}\mathbf{u} - p\mathbf{n}, \nu\partial_{\mathbf{n}}\boldsymbol{\varphi} + \psi\mathbf{n}\rangle_{\partial\Omega} - \frac{\delta}{\mu+\delta}\,\langle \mathbf{u} - \mathbf{q}_D, \nu\partial_{\mathbf{n}}\boldsymbol{\varphi} + \psi\mathbf{n}\rangle_{\partial\Omega} \\ + \frac{\mu\delta}{2(\mu+\delta)}\,\langle (\mathbf{u}\cdot\mathbf{n})\mathbf{u}, \nu\partial_{\mathbf{n}}\boldsymbol{\varphi} + \psi\mathbf{n}\rangle_{\partial\Omega} = 0 \end{aligned} \tag{35}$$

Adding the weak formulation and Eqs. (34) and (35) we obtain directly Eq. (33). □

5.4 Comments on Stabilisation Techniques

The presented numerical scheme is unstable with respect to two different sources, namely the convection dominance of the convection-diffusion equation or the Navier-Stokes system for large Reynolds numbers and the lack of inf-sub stability, due to the specific choice of the finite element spaces for the velocity and pressure components in the Navier-Stokes system. We can overcome both issues by using

the so called local projection stabilisation. We briefly comment on the technique and cite further literature.

5.4.1 Convection Stabilisation

We use a method for the convection stabilisation, which was introduced by Becker et al. [5]. For the model problem

$$(u_h, \varphi_h) + ((\boldsymbol{\beta} \cdot \nabla)\, u_h, \varphi_h) = (f, \varphi) \qquad \forall \varphi \in V_h,$$

we add hereby the stabilisation term

$$s(u_h, \varphi_h) = s_{\mathrm{LPS}}(u_h, \varphi_h) := \sum_{T \in \mathscr{T}_h} \delta_T \left(\pi_h \left(\boldsymbol{\beta} \cdot \nabla u_h\right), \pi_h \left(\boldsymbol{\beta} \cdot \nabla \varphi\right)\right).$$

The operator $\pi_h = I - \mathscr{P}_{2h}$ consists of the difference of the identity operator and a projection operator

$$\mathscr{P}_{2h} : V_h \to V_{2h}$$

defining a mapping of the current trial function space V_h onto the coarser one V_{2h}. The so defined mapping measures fluctuation of the convection term. The parameter δ_T is chosen as follows

$$\delta_T = \delta_0 \frac{h}{k\theta|\boldsymbol{\beta}|}.$$

This stabilisation scheme admits in principle the same properties in terms of stability and accuracy as the SUPG scheme. An import advantage is that for this scheme again the principles 'optimise-then-discretise' and 'discretise-then-optimise' are interchangeable.

5.4.2 Pressure Stabilisation

For computational simplicity we work with bilinear finite elements for both the pressure and the velocity approximation. That means $V_h = \hat{V}_h^2$ for the discrete velocity space and $M_h = \hat{V}_h$ for the discrete pressure space with $\hat{V}_h$ defined as in Eq. (17). It is well known that the inf-sup condition

$$\min_{\mu_h \in M_h} \left(\max_{\boldsymbol{\varphi}_h \in V_h} \frac{-(\mu_h, \nabla \cdot \boldsymbol{\varphi}_h)}{\|\boldsymbol{\varphi}_h\|_{V_h} \|\mu_h\|_{M_h}} \right) \geq \gamma_h \geq \gamma > 0$$

for this particular choice is violated.

We can also use the mentioned local projection stabilisation technique to stabilise our approach related to inf-sup-instability as it is presented in the work of Becker et al. [4].

We add therefore the bilinear form

$$s_{\mathrm{LPS}}(\{\mathbf{u}_h, p_h\}, \{\boldsymbol{\varphi}_h, \mu_h\}) = \sum_{T \in \mathscr{T}_h} \alpha_T \left(\nabla(\pi_h p_h), \nabla(\pi_h \mu_h)\right)_T$$

to the left hand side of the divergence equation

$$(\mu_h, \nabla \cdot \mathbf{u}_h) = 0 \qquad \forall \mu_h \in M_h,$$

where π_h denotes again the fluctuation operator defined as in the case of the convection stabilisation. The parameter is chosen as suggested in the literature as

$$\alpha_T = \frac{h_T^2}{\nu}.$$

6 Numerical Results

We will use a few test cases to exemplify the functionality of the presented method. Although the theory was already developed for the use of the fully nonlinear Navier-Stokes equations, we avoid at first to work with high Reynolds-numbers and suppress the time-dependent character of the flow equations in the first two test cases. The reason for this is that our main objective is to prove that we can estimate reliable boundary conditions for the flow field and the intensity function by only sparsely given data. Afterwards, we will in a third test case apply the method to identify a fluid flow, which is described by the fully non-linear and time-dependent Navier-Stokes system, which emphasises especially the usage of the high-fidelity physical model in the proposed identification method.

In the first two examples we use in principle the same setting. The computational domain and the time horizon are given by

$$\Omega = (0, 1) \times (0, 1), \qquad \mathscr{T} = (0, 0.2].$$

Furthermore we set

$$\varepsilon = 10^{-10}, \qquad \text{and } \nu = 1.$$

All numerical calculations are performed on a mesh with 289 spatial nodes and 40 time steps.

6.1 First Test Data Set

The first test data set was already presented in the introduction in Fig. 1. It consists of three intensity functions $\mathscr{I}_1$, $\mathscr{I}_2$ and $\mathscr{I}_3$ representing a brightness distribution in form of a bulb signal. The first function shows the bulb signal at the initial time $t = 0$, the second function shows the signal after a movement with the constant flow field $\beta = (0, 2)^T$ at the intermediate time point $t = 0.1$ and the third function shows the transported signal at the end time point.

We performed then the approach from the Definitions 3 and 4 for the parameter choice

$$\mu_1 = \mu_2 = h$$

with the cell diameter h.

The method is for small values of the regularisation parameter α very unstable unless we have a good initial value for the time dependent boundary functions q_I and $\mathbf{q_u}$. The reason for this is that we solve in general an inverse problem that requires a certain regularisation (see Engl et al. [14]).

Thus we use a homotopy method in α, by solving the optimisation problem for a large α_k and then taking $q_I^{(k)}$ and $\mathbf{q}_\mathbf{u}^{(k)}$ as initial values for a further solution of the optimisation problem with a reduced $\alpha_{k+1} = \sigma\alpha_k$ with $\sigma \in (0, 0.5)$. After a few steps of this technique we obtain the reconstruction $I_{k,h}$ presented in Fig. 4. The regularisation parameter was around 10^{-2} and the final Newton residual was approximately 10^{-5}.

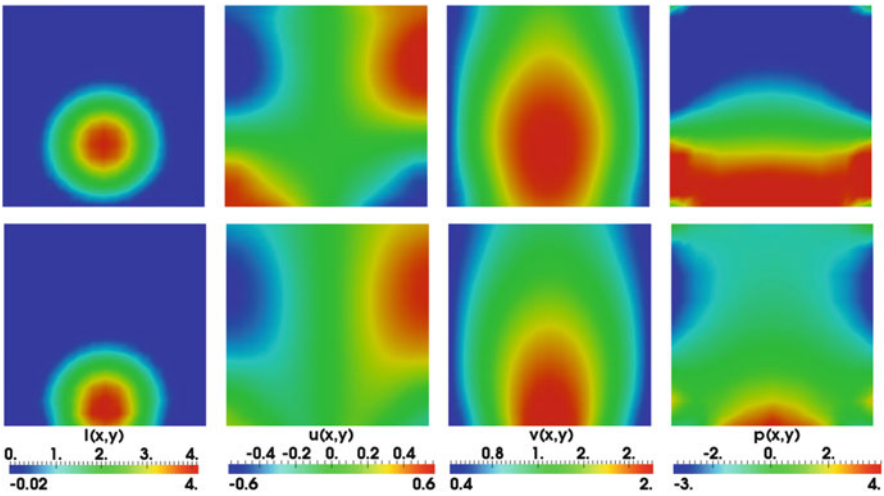

Fig. 4 From *left* to *right*: $I(\mathbf{x})$, $u(\mathbf{x})$, $v(\mathbf{x})$ and $p(\mathbf{x})$. *Top*: $t = \frac{3T}{4}$. *Bottom*: $t = \frac{T}{4}$. Regularisation parameter: $\approx \alpha = 10^{-2}$. $\|I_{k,h} - \hat{I}\|^2_{L^2(0,T;L^2(\Omega))} = 5.01 \cdot 10^{-4}$

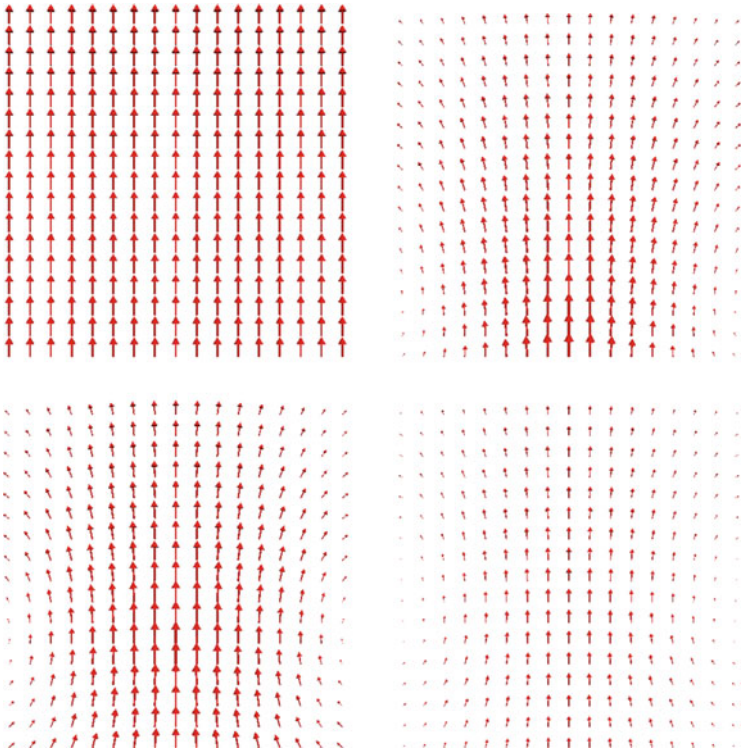

Fig. 5 *Top left*: $\boldsymbol{\beta} = (0, 2)^T$. *Top right*: $\mathbf{u}_h$ at $t = \frac{T}{4}$. *Bottom left*: $\mathbf{u}_h$ at $t = \frac{3T}{4}$. *Bottom right*: $\mathbf{u}_h$ at $t = T$

The bottom row shows the brightness function I, the x- and y-component of the transport field and the associated pressure function (from left to right) for the time $t = \frac{T}{4}$. The top row shows the same functions for the time $t = \frac{3T}{4}$. We see that the signal is transported appropriately over the boundary and that within the area, where the signal is different from zero also the estimation of the flow field seems to be a good approximation of the expected field (see therefore also Fig. 5).

Furthermore, we compared the computed intensity function to the expected one in terms of the L^2-norm, which is a time continuous version of the data term:

$$\|I_{k,h} - \hat{I}\|^2_{L^2(0,T;L^2(\Omega))} = 5.01 \cdot 10^{-4} \qquad (\|\hat{I}\|^2_{L^2(0,T;L^2(\Omega))} = 2.48 \cdot 10^{-1}).$$

However, this good looking result is only a coincidence, due to the simple situation of our test case. Since we assumed the underlying transport field to be constant the special choice of our regularisation term leads to an appropriate recovering of the time-dependent function $I(\mathbf{x}, t)$. In general there are infinitely many solenoidal flow fields that generate the three given intensity functions $\mathscr{I}_1$, $\mathscr{I}_2$ and $\mathscr{I}_3$ (e.g. $\beta_c(\mathbf{x}, t) = \sin^c\left(\frac{t\pi}{T}\right)(0, 2)^T$), which we used as data in the optimisation

problem. All of these flow fields lead to completely different intensity functions (e.g. $I_{\beta_c}(\mathbf{x}, t)$). Thus, it is impossible to reconstruct a specific flow field, without introducing further a priori knowledge about the flow field in the optimisation process. This consideration emphasises again the ill-posed character of the problem and shows that we have to be careful in trusting the reconstruction of fluid flow fields, without additional information about this fields.

Nevertheless, we can use the method as an interpolator between discrete intensity functions as the next test case indicates.

6.2 Second Test Data Set

The second test case was also mentioned in the introduction and consists of the six brightness functions presented in Fig. 2 at the time points $t = 0.04(k-1)$ with $k = 1, \ldots, 6$. The underlying transport field for the movement is

$$\boldsymbol{\beta}(\mathbf{x}, t) = \frac{5\pi}{2}(-y, x)^T.$$

Obviously the signal is throughout the image sequence transported from the lower boundary to the left boundary. Thus, we initialise our computational method this time by the following assumption of the transport field

$$\mathbf{u}^0(\mathbf{x}) = (-2, 2)^T,$$

since this field describes the principle direction of the flow. Afterwards, we solve as in the first test case the optimisation problem with

$$\mu_1 = \mu_2 = h.$$

The result of this calculation is visualised in Fig. 6. We want to emphasise that we choose time points for the visualisation in which no data is available to make clear that this method interpolates intermediate brightness distributions. Our next aim is to compare different parameter choices for the boundary control formulation. We use therefore four different cases. The first three cases are given as follows

$$\begin{aligned} \mu_1 &= \mu_2 = 1, && \text{(Case 1)} \\ \mu_1 &= \mu_2 = 0.1, && \text{(Case 2)} \\ \mu_1 &= \mu_2 = h, && \text{(Case 3)} \end{aligned}$$

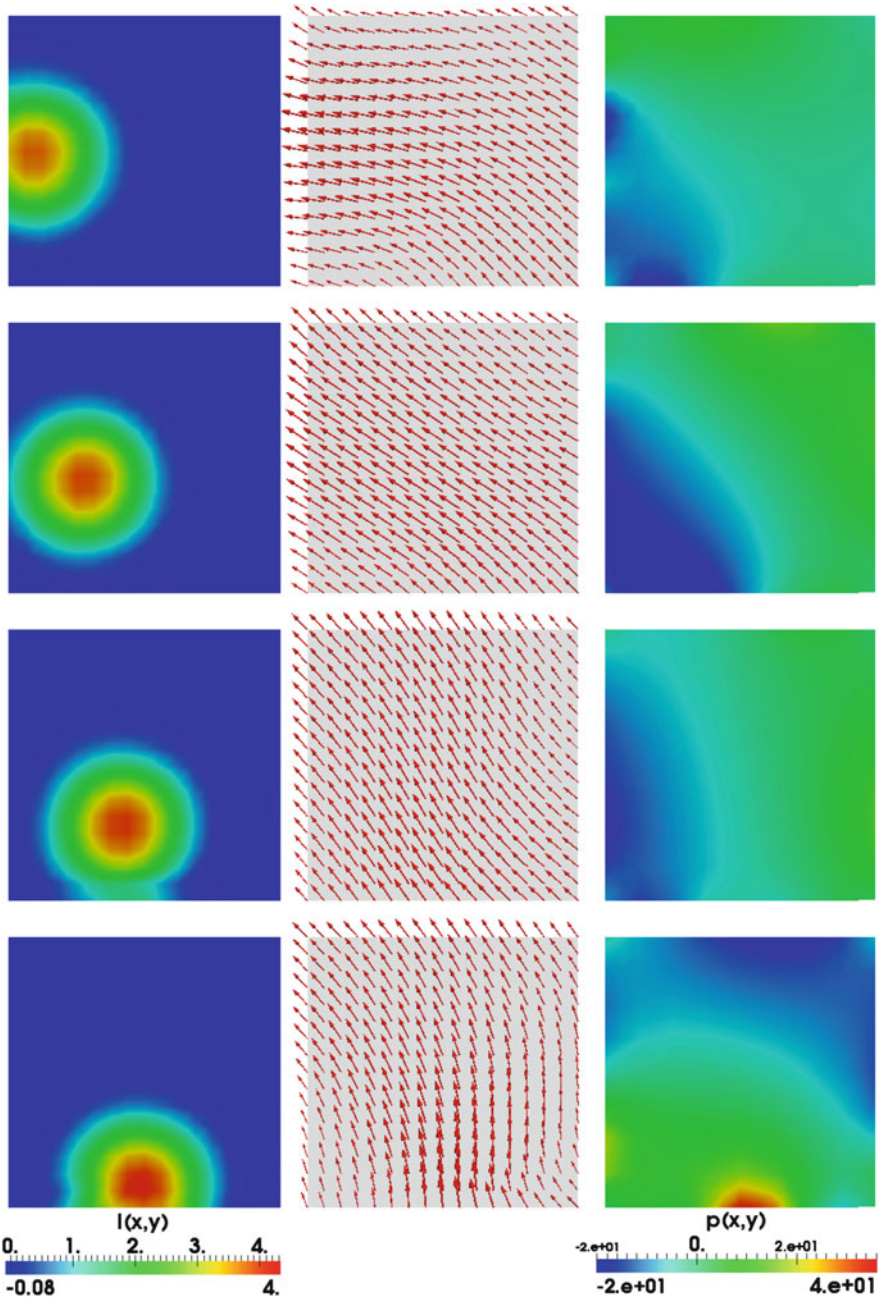

Fig. 6 Calculated solution for $\alpha \approx 10^{-3}$. *Left column*: from *bottom to top*: $I(\mathbf{x}, t_k)$ with $t_k = \frac{kT}{8}$ and $k = 1, 3, 5, 7$. *Middle column*: corresponding transport field. *Right column*: corresponding pressure function

Table 1 We indicate the error between the expected brightness function in time and the calculation by $e_{h,k} := \|I - I_{h,k}\|^2_{L^2(\Omega\times[0,2])}$. The expected brightness function has the following norm $g := \|I\|^2_{L^2(\Omega\times[0,2])} = 2.454 \cdot 10^{-1}$

Case	$e_{h,k}$	Rel. Error ($\frac{e_{h,k}}{g}$) (%)
1	$1.735 \cdot 10^{-3}$	0.71
2	$7.976 \cdot 10^{-4}$	0.33
3	$6.205 \cdot 10^{-4}$	0.25
4	$5.616 \cdot 10^{-4}$	0.23
5	$5.346 \cdot 10^{-4}$	0.22

for the parameters in the Definitions 3 and 4. For the final test case we want to set $\mu = 0$. Thus, we use instead of the usual boundary bilinear forms in the two definitions the stabilised ones in Eq. (32) for the Navier-Stokes part and Eq. (25) for the part of the physic-based optical flow equation

$$\mu_1 = \mu_2 = 0, \qquad \text{Eq. (32) with } \gamma(h) := \frac{h}{5} \text{ and Eq. (25)} \qquad \text{(Case 4)}.$$

We want to emphasise that these two conditions implement Dirichlet boundary controls for which the developed theory could not be applied.

The results of the calculations are shown in Table 1. Here we document the ability of the method to recover the expected movement of the bulb signal during the whole time horizon in terms of the L^2-error. The table shows that for $\mu = 1$ the method is worse than for small choices of μ or even for a implemented weak Dirichlet condition. The reason for this is that artefacts on the inflow boundary occur for the recovery of the signal. Thus, it seems to be a good idea to work with the weak Dirichlet conditions.

Unfortunately, the solution has then another drawback since the transport field is no longer continuous in time as Fig. 7 indicates. The left column represents the transport field in the case of the weak Dirichlet controls. As we can see the field is immediately changing after the time stepping scheme passing a time point, where a brightness function information is available. Hence, the field has some kind of jump with respect to the time variable. We want to emphasise that this is nothing unexpected, since the theory is not working in this case and we cannot expect the same temporal regularity as in the case of Robin controls.

As a result of the discussion we propose a "trade-off" version of the used methods. Here we use the Robin-type control for the Navier-Stokes part with $\mu_1 = h$ and the Dirichlet control in Eq. (25) for the brightness function. This leads to a method which smoothly transports the signal across the boundary by a temporally smooth transport field. We document the error of this combination by "Case 5" in Table 1.

However, the last two examples rely on temporal constant solenoidal fields, which could also be solutions of the steady Stokes equations. Thus, the spent effort for interpolating discrete image intensities with our approach basing on a

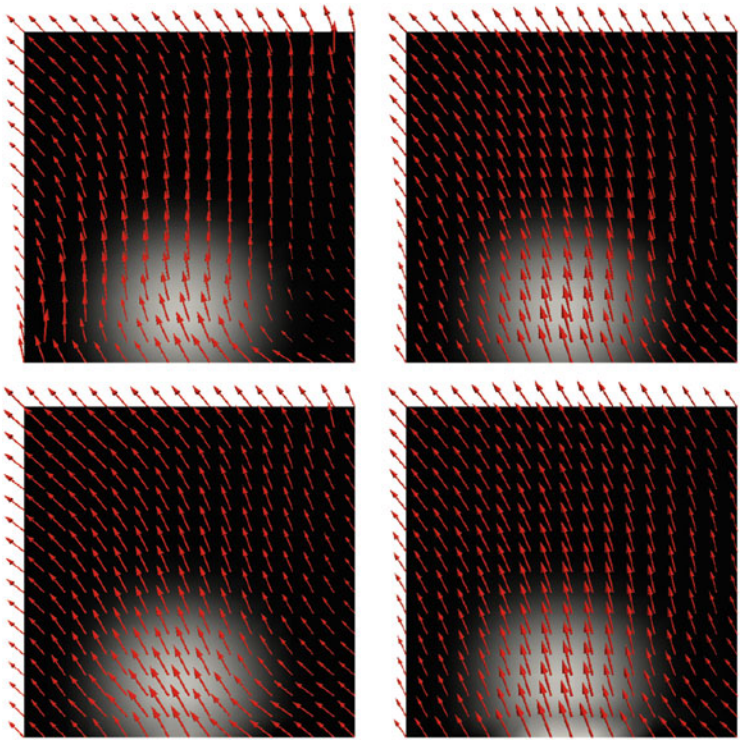

Fig. 7 *Top*: $t = 0.04$. *Bottom*: $t = 0.0425$. *Left column*: transport field for the weak Dirichlet boundary control. *Right column*: transport field for the Robin-type control approach with $\mu_1 = \mu_2 = 0.1$. The left transport field is immediately changing and has therefore a kink in the time variable

regularisation with a fully time-dependent and non-linear physical model for the fluid flow is questionable. To justify the reliability of our consideration we present a final test case, which based on observations of a dynamic flow.

6.3 Third Test Data Set

The following example relies on the sequence $\mathscr{I}_k$ presented in Fig. 3, which was obtained after executing a forward calculation of system (1). We will therefore shortly present the generation of the image sequence. The computational domain is (Fig. 8)

$$\Theta = (-0.01m, 0.19m) \times (0, 0.1m).$$

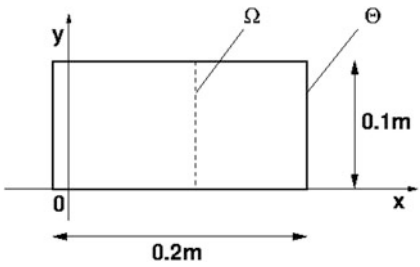

Fig. 8 The image domain $\Omega = (0, 0.1m)^2$ is an aperture of the original computational domain $\Theta = (-0.01m, 0.19m) \times (0, 0.1m)$

The time horizon is $(0, 3s]$. We prescribe no-slip boundary conditions on the upper and lower boundary. The left boundary is an inflow boundary, while on the right boundary the outflow occurs. The inflow is described by the function

$$\mathbf{u}(\mathbf{x}, t) := (10 \min(t, 1) \max(0, \omega(x, y)), 0)^T$$

with

$$\omega(x, y) := \frac{1}{4}\left(y - \left(\frac{1}{4} + \frac{1}{5}\sin(\pi t)\right)\right) \cdot \left(\left(\frac{3}{4} + \frac{1}{5}\sin(\pi t)\right) - y\right)\frac{m}{s}.$$

Furthermore, we choose a kinematic viscosity $\nu = 0.01\frac{m^2}{s}$. Finally, the passive tracer is also introduced by a Dirichlet-type boundary condition on the left side of the domain Θ:

$$I(\mathbf{x}, t) := \max(\cos(\pi t), 0).$$

For the diffusivity parameter in the convection-diffusion equation of the tracer we choose $\varepsilon = 1e - 10$.

Then we perform a calculation with 60 steps of an implicit Euler method in time and with a spatial discretisation into 2145 grid points of a regular mesh. Thus, we obtain the reference solutions $\mathbf{u}_r$ and I_r. By using $I_r(\mathbf{x}, t_k)$ for $\mathbf{x} \in \Omega = (0, 0.1m)^2$ we generate afterwards three different "image sequences" on the aperture domain Ω. Each sequence represents a different sampling rate for the images:

$$\begin{aligned}
\mathscr{I}^{(1)} &:= I_r(\mathbf{x}, t_k), && \text{with } t_k = 0.05k, && k = 0, \ldots, 60,\\
\mathscr{I}^{(2)} &:= I_r(\mathbf{x}, t_k), && \text{with } t_k = 0.25k, && k = 0, \ldots, 12,\\
\mathscr{I}^{(3)} &:= I_r(\mathbf{x}, t_k), && \text{with } t_k = 0.5k, && k = 0, \ldots, 6.
\end{aligned}$$

We have a clear difference between sampling rate and time discretisation in the sequences $\mathscr{I}^{(2)}$ and $\mathscr{I}^{(3)}$, while for $\mathscr{I}^{(1)}$ the sampling rate and the time discretisation coincides.

These sequences are used for the reconstruction of the flow on the aperture domain Ω. Therefore, we use our Robin-boundary control approach with the following settings. From the image sequences we observe a starting phase of the flow and a movement from left to right of the image patterns. Thus, we set

$$\mathbf{g}(\mathbf{x}, t) := (\min(t, 1) u_{\max} y(1 - y), 0)^T \frac{m}{s}$$

and using instead the modified function

$$\tilde{\mathbf{q}}_{\mathbf{u}}(\mathbf{x}, t) := \mathbf{q}_{\mathbf{u}}(\mathbf{x}, t) + \mathbf{g}(\mathbf{x}, t)$$

in the Robin-boundary formulation [cf. fourth equation in (5)]. The parameter $u_{\max}$ can also be roughly estimated by the given images. We choose $u_{\max} = 2$.

To initialise also the inflow of signals I across the inflow boundary on the left we choose a linear interpolation between the given discrete image signals of the sequences on the boundary. We denote this interpolated function by $\mathfrak{I}(\mathscr{I}^{(j)})(\mathbf{x}, t)$ with $i = 1, 2, 3$ and have thus the modified function

$$\tilde{q}_I := \mathfrak{I}(\mathscr{I}^{(j)})(\mathbf{x}, t) + q_I$$

in the Robin-boundary formulation [cf. third equation in (5)]. For the parameter in the Navier-Stokes part we choose this time $\mu_1 = 1$ and perform a weak Dirichlet control in the fashion of Eq. (25) as in the test case before for the convection-diffusion equation part.

This time we will work with two different values for α_1 and α_2 in the cost functional (see Definition 1). The reason for this is that we want to penalise too big changes of the image function on the boundary since we assume that the linear interpolated boundary conditions of the image sequence data is already a qualitative approximation of the effective boundary conditions. Thus, the α_1-term has more the character of a correction. However, since we have no clue about the boundary conditions for the fluid flow we want to choose α_2 as small as possible. As in the test cases before we apply therefore a homotopy-type method that stops, when α_2 drops below a threshold Tol. Our experiences shows that $\alpha_1 = 100$ and $\text{Tol} = 10^{-3}$ is an appropriate choice, when we additionally weighting the data term in the cost functional by a factor 100.

The results for the identification by this settings are presented in Fig. 9 (Magnitude of the flow field) and Fig. 10 (Intensity function) for the time points $t_1 = 0.75$ (Row A), $t_2 = 1.5$ (Row B), $t_3 = 2.25$ (Row C) and $t_4 = 3$ (Row D). From left to right we visualise in the both figures the expected solution (Column 1), the results for sequence $\mathscr{I}^{(1)}$ (Column 2), $\mathscr{I}^{(2)}$ (Column 3) and $\mathscr{I}^{(3)}$ (Column 4). For a more qualitative comparison we investigate the following quantity of interest

$$\eta(t) := \|\mathbf{u}(t) \cdot \nabla I(t)\|_2^2.$$

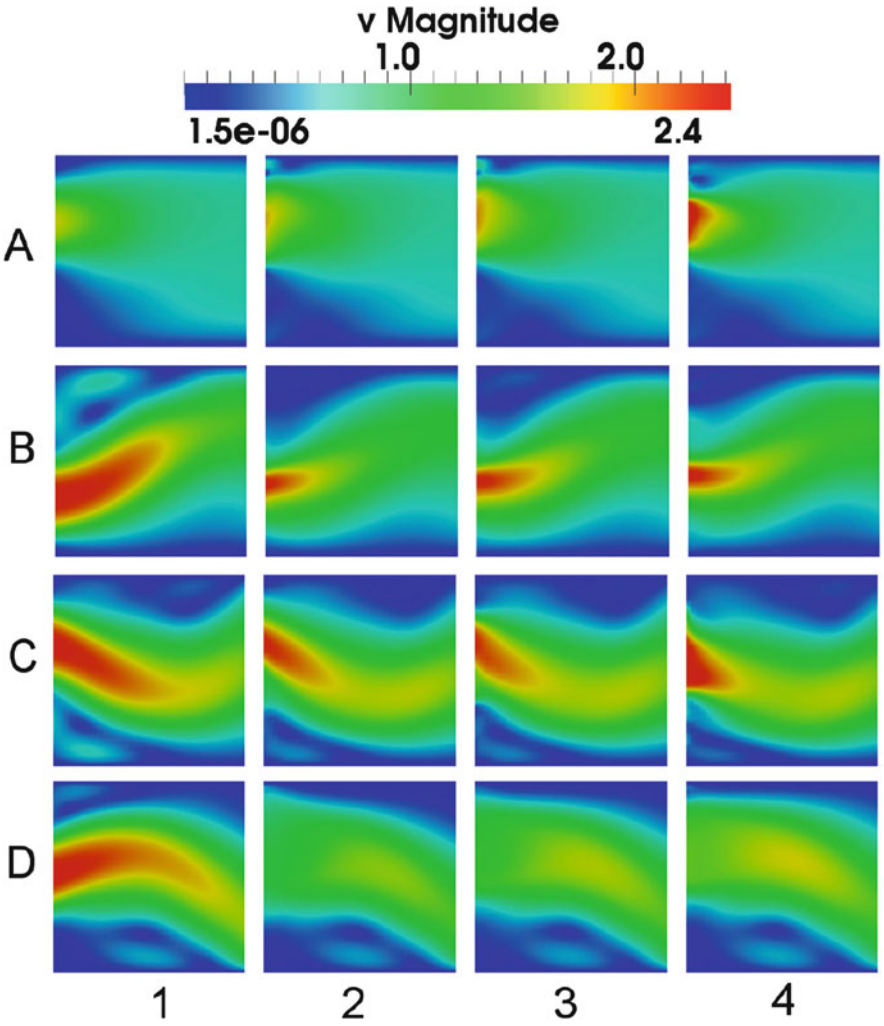

Fig. 9 Comparison of the identified fluid flow in terms of the magnitude of the flow field. Row A to row D: $t_k = 0.75k$ with $k = 1, \ldots, 4$. Columns from *left* to *right*: expected (1), $\mathscr{I}^{(1)}$ (2), $\mathscr{I}^{(2)}$ (3) and $\mathscr{I}^{(3)}$ (4)

This quantity has the feature that it depreciate the recovery in areas where the intensity is nearly constant. The evolution of the $\eta(t)$ across the mentioned time interval is documented in Fig. 11. The left picture shows the expected curve (blue), the estimation with the data from sequence $\mathscr{I}^{(1)}$ (green dashed) and the results of a forward calculation with $\mathbf{g}(\mathbf{x}, t)$ and $\mathfrak{I}(\mathscr{I}^{(j)})$ (red dash-dotted). We see a clear improvement by the usage of our identification process. In the left picture of

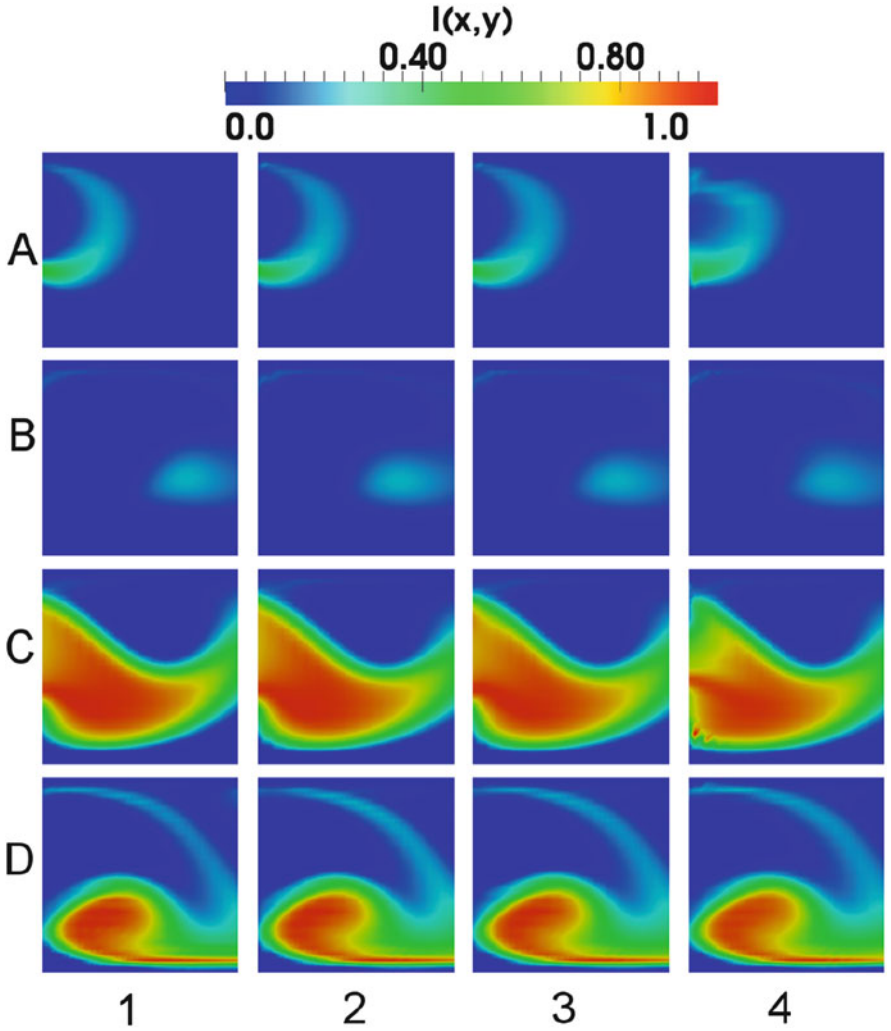

Fig. 10 Comparison of the reconstructed intensity functions. Row A to row D: $t_k = 0.75k$ with $k = 1, \ldots, 4$. Columns from *left* to *right*: expected (1), $\mathscr{I}^{(1)}$ (2), $\mathscr{I}^{(2)}$ (3) and $\mathscr{I}^{(3)}$ (4)

Fig. 11 we compared the quality of the reconstruction in terms of the three data sequences $\mathscr{I}^{(1)}$ (green), $\mathscr{I}^{(2)}$ (blue dashed) and $\mathscr{I}^{(3)}$ (red dash-dotted). As expected we see a clear improvement by using as much data as possible. However, the result also indicates that we are not able to fit the curve even if we have image data in every time step of our temporal discretisation. The reason for this is the ill-posed character of the problem.

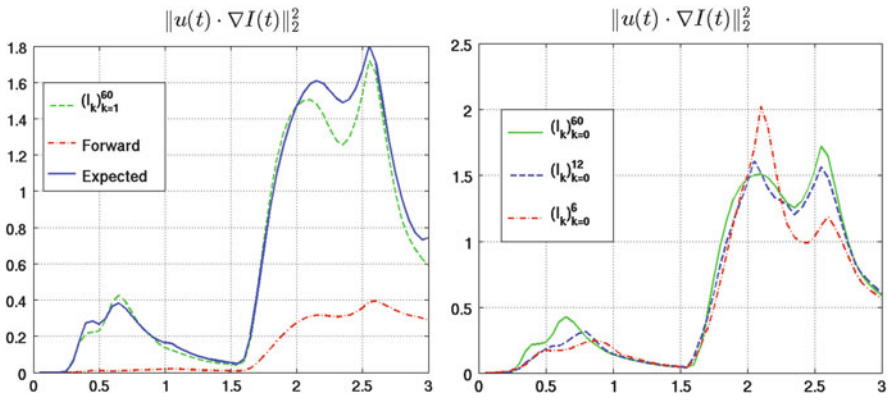

Fig. 11 Recovery of the quantity of interest $\eta(t)$ by our approach. *Left*: comparison of the expected curve (*blue*), identification with intensity informations in each time step (*green*) and a forward calculation (*red*). *Right*: different data sequences: $\mathscr{I}^{(1)}$ (*green*), $\mathscr{I}^{(2)}$ (*blue*) and $\mathscr{I}^{(3)}$ (*red*)

7 Discussion on the Application of Multiple Shooting Methods

The numerical solution of the presented optimisation problem relies on a Newton-type method developed by Becker et al. [6] to find a solution of the optimality system, which can be introduced by means of the Lagrangian [see Eq. (13)].

We observed for all our calculations that the method's performance is very sensitive with respect to the choice of the initial values for the control variables q_I, $\mathbf{q_u}$, the length of the time horizon and the chosen regularisation parameter.

As mentioned in the last section we used a homotopy method in α to be able to solve the problem in a stable way for small values of the regularisation parameter. We want to remark that for each step of the homotopy method a whole optimisation problem must be solved, which increases the computational costs immensely.

However, the unstable behaviour is probably a result of the structure of the PDE-constrained optimisation problem. We remember therefore the cost functional in Definition 1

$$J(q_I, \mathbf{q_u}, I)$$

which is minimised with respect to the weak formulation of the state equation in Definition 4. The latter is now converted into the following abstract form

$$((\partial_t I, \psi)) + \bar{a}(\mathbf{u}; I, \psi) + \bar{b}(q_I, \psi) + (I(0) - \mathscr{I}_1, \psi(0)) = 0 \qquad \forall \psi \in \mathscr{X}_I$$

$$((\partial_t \mathbf{u}, \boldsymbol{\varphi})) + \bar{c}(\mathbf{u})(\boldsymbol{\varphi}) + \bar{d}(\mathbf{q_u}, \boldsymbol{\varphi}) + \big(\mathbf{u}(0) - \mathbf{u}^0, \boldsymbol{\varphi}(0)\big) = 0 \qquad \forall \boldsymbol{\varphi} \in \mathscr{X}_{\mathbf{u}}$$

with the linear forms $\bar{a}(\cdot;\cdot,\cdot)$, $\bar{b}(\cdot,\cdot)$, $\bar{c}(\cdot)(\cdot)$ and $\bar{d}(\cdot)(\cdot)$ containing the terms of the forms in Eq. (5) integrated over the time interval $[0,T]$. Here we separated the control terms from the rest of the equation.

We concretise the Lagrangian

$$\begin{aligned}\mathscr{L}(q_I,\mathbf{q_u},I,\mathbf{u},K,\mathbf{z}) := \; & J(q_I,\mathbf{q_u},I) + (\!(\partial_t I,K)\!) + \bar{a}(\mathbf{u};I,K) + \bar{b}(q_I,K) \\ & + (I(0)-\mathscr{I}_1,K(0)) + (\!(\partial_t\mathbf{u},\mathbf{z})\!) + \bar{c}(\mathbf{u})(\mathbf{z}) + \bar{d}(\mathbf{q_u},\mathbf{z}) \\ & + \left(\mathbf{u}(0)-\mathbf{u}^0,\mathbf{z}(0)\right).\end{aligned}$$

With the Lagrangian we can obtain the mentioned optimality system, which consists of the state equations

$$\begin{aligned}\mathscr{L}_K(q_I,\mathbf{q_u},I,\mathbf{u},K,\mathbf{z})(\delta K) &= 0, \qquad \forall \delta K \in \mathscr{X}_I, \\ \mathscr{L}_{\mathbf{z}}(q_I,\mathbf{q_u},I,\mathbf{u},K,\mathbf{z})(\delta \mathbf{z}) &= 0, \qquad \forall \delta \mathbf{z} \in \mathscr{X}_{\mathbf{u}},\end{aligned}$$

adjoint equations

$$\begin{aligned}\mathscr{L}_I(q_I,\mathbf{q_u},I,\mathbf{u},K,\mathbf{z})(\delta I) &= 0, \qquad \forall \delta I \in \mathscr{X}_I, \\ \mathscr{L}_{\mathbf{u}}(q_I,\mathbf{q_u},I,\mathbf{u},K,\mathbf{z})(\delta \mathbf{u}) &= 0, \qquad \forall \delta \mathbf{u} \in \mathscr{X}_{\mathbf{u}},\end{aligned}$$

and control equations

$$\begin{aligned}\mathscr{L}_{q_I}(q_I,\mathbf{q_u},I,\mathbf{u},K,\mathbf{z})(\delta q_I) &= 0, \qquad \forall \delta q_I \in \mathscr{Q}_I, \\ \mathscr{L}_{\mathbf{q_u}}(q_I,\mathbf{q_u},I,\mathbf{u},K,\mathbf{z})(\delta \mathbf{q_u}) &= 0, \qquad \forall \delta \mathbf{q_u} \in \mathscr{Q}_{\mathbf{u}}.\end{aligned}$$

The last two conditions can be used to substitute the control variables by the adjoint variables in the state equation. Collecting afterwards the state and the adjoint variables by the overall vector $\mathbf{x} := \{I,\mathbf{u},K,\mathbf{z}\}$ we can summarise the optimality system by the abstract system of equations

$$\begin{aligned}\partial_t \mathbf{x}(t) &= \mathscr{A}(\mathbf{x}(t)), \qquad \forall t \in [0,T], \\ \hat{\mathbf{g}}(\mathbf{x}(0),\mathbf{x}(T)) &:= B_0\mathbf{x}(0) + B_T\mathbf{x}(T) - (\mathscr{I}_1,\mathbf{u}^0,I(T)-\mathscr{I}_N,0)^T = 0\end{aligned} \tag{36}$$

with

$$B_0 = \begin{pmatrix}\mathbf{I} & \mathbf{0} \\ \mathbf{0} & \mathbf{0}\end{pmatrix}, \qquad B_T = \begin{pmatrix}\mathbf{0} & \mathbf{0} \\ \mathbf{0} & \mathbf{I}\end{pmatrix}, \qquad \text{and } \mathbf{I} = \begin{pmatrix}1 & 0 \\ 0 & 1\end{pmatrix},$$

and an abstract differential operator $\mathscr{A}$. It is known that the above abstract problem represents a boundary value problem (BVP) for the state and adjoint variables, with respect to given values for the state variables I and $\mathbf{u}$ at the initial time and for the

adjoint variables K and $\mathbf{z}$ at the end time point (cf. Carraro et al. [12] for optimal control problems with parabolic PDE constraints).

This is a possible explanation for the instability of our sophisticated PDE-constrained optimisation problem, especially if we consider long time horizons, as it was figured out in the article of Weiss [40] for a much simpler configuration. To follow this argumentation we discretise system (36) on a fixed spatial grid by the method of lines:

$$\begin{aligned} \mathbf{x}_h'(t) &= \hat{\mathbf{f}}_h\left(t, \mathbf{x}_h(t)\right), \qquad \forall t \in [0, T], \\ \hat{\mathbf{g}}_h\left(\mathbf{x}_h(0), \mathbf{x}_h(T)\right) &= 0. \end{aligned}$$

The resulting system is a classical ODE-based BVP. Weiss showed that for such problems multiple shooting increases the size of the domain within which we may choose the initial value for a successful performance of Newton's method. However, whether working with multiple shooting is reliable requires a further detailed mathematical and numerical investigation. First steps towards the application of multiple shooting methods to parabolic optimal control problems were presented by Carraro et al. [11, 12], Hesse et al. [21] and Potschka [34].

Since our PDE-constrained optimisation problem could also be interpreted as a parabolic boundary control problem, it would be an interesting topic for further research to apply the rather technical multiple shooting method to our highly complex problems. We conjecture that it is possible, due to the stabilising effect of the multiple shooting method, to reduce the effort of the homotopy method in α.

Another big advantage of multiple shooting methods is that they are well suited for parallelisation. This could also clearly accelerate the solution process in terms of needed computational time.

8 Conclusion

In this contribution we suggested a PDE-constrained optimisation problem based on the estimation of boundary functions, which can be used in a certain physical setting to evaluate a flow field transporting a passive tracer across the computational domain boundaries. The only available data is a temporally sparse sequence of measurements of the intensity function of a passive tracer. The motivation for the investigation is the increasing use of image processing, especially optical flow estimation, techniques in fluid flow evaluation.

However our main objective was to formulate a mathematically well-posed problem, which is also easy to handle from the computational point of view. We suggested therefore a Robin-type control formulation, since in simple linear settings a close connection to Dirichlet control problems was observed. Although our Robin-type approach is well-posed and has a straightforward computational treatment, we have not enhanced the theory for approximating Dirichlet controls by Robin-type

controls to our system. On the one hand, it is not necessary to work with Dirichlet controls for our identification purposes. On the other hand we have no appropriate very weak formulation of the problem. Here we see a possible direction for further theoretical research to connect Robin-type and Dirichlet controls also for such sophisticated coupled systems of equations.

We proved the functionality of the method based on synthetic test cases. We were able to interpolate a sparsely given image sequence, without the knowledge of the underlying flow field, even when the information on the intensity function moved across the boundary. However the examples were too simple to prove the necessity of using the fully nonlinear Navier-Stokes equations. Applying the method to more realistic prototypical examples or real world problems would be a further step for our work.

For all our numerical calculations we enhanced a generalisation for weakly imposed boundary conditions suggested by Juntunen et al. [24] to the class of PDEs we have to deal with and used them for our numerical calculations.

Acknowledgements This article is based on collaboration with Prof. Dr. Dr. h.c. R. Rannacher (IAM, Heidelberg University) and Priv.-Doz. Dr. C.S. Garbe (IPM, Heidelberg University). Furthermore M. Geiger and Dr. T. Carraro (both IAM, Heidelberg University) supported the author to connect the content to the time decomposition topic in the conclusions. The author gratefully acknowledges all mentioned persons for many fruitful discussions and for their support.

References

1. Bachl, F., Garbe, C., Fieguth, P.: A Bayesian approach to apaceborn hyperspectral optical flow estimation on dust aerosols. In: Geoscience and Remote Sensing Symposium (IGARSS), pp. 256–259 (2012)
2. Bachl, F., Garbe, C., Fieguth, P.: Baysian inference on integrated continuity fluid flows and their application to dust aerosols. In: Geoscience and Remote Sensing Symposium (IGARSS), pp. 2246–2249 (2013)
3. Becker, R.: Mesh adaptation for Dirichlet flow control via Nitsche's method. Commun. Numer. Meth. Eng. **18**(9), 669–680 (2002)
4. Becker, R., Braack, M.: A finite element pressure gradient stabilization for the Stokes equations based on local projections. Calcolo **38**(4), 173–199 (2001)
5. Becker, R., Braack, M.: A two-level stabilization scheme for the Navier-Stokes equations. In: Proceedings of ENUMATH (2003)
6. Becker, R., Meidner, M., Vexler, B.: RoDoBo: A C++ Library for Optimization with Stationary and Nonstationary PDEs. Institute of Applied Mathematics, Heidelberg University, Heidelberg. http://www.rodobo.org (2005)
7. Belgacem, F., Fekih, H., Metoui, H.: Singular pertubation for the Dirichlet boundary control of elliptic problems. ESAIM **37**(5), 833–850 (2003)
8. Borzi, A., Ito, K., Kunisch, K.: Optimal control formulation for determining optical flow. SIAM J. Sci. Comput. **24(3)**, 818–847 (2002)
9. Braess, D.: Finite Elemente, vol. 4. Springer, Berlin (2007)
10. Brenner, S., Scott, L.: The Mathematical Theory of the Finite Element Method, vol. 3. Springer, Berlin (2007)

11. Carraro, T., Geiger, M.: Direct and indirect multiple shooting for parabolic optimal control problems. In: Thomas, C., Michael, G., Stefan, K., Rolf, R. (eds.) Multiple Shooting and Time Domain Decomposition Methods. Springer, Heidelberg (2015, in this issue)
12. Carraro, T., Geiger, M., Rannacher, R.: Indirect multiple shooting for nonlinear parabolic optimal control problems with control constraints. SIAM J. Sci. Comput. **36**(2), 452–481 (2014)
13. Chen, K., Lorenz, D.: Image sequence interpolation based on optical flow, image segmentation and optimal control. IEEE Trans. Image Process. **21**(3), 1020–1030 (2012)
14. Engl, H., Hanke, M., Neubauer, A.: Regularization of Inverse Problems. Kluwer Academic, Dordrecht (2000)
15. Evans, L: Partial Differential Equations, 2nd edn. American Mathematical Society, Providence, RI (2010)
16. Farwig, R., Kozono, H., Sohr, H.: Very weak, weak and strong solutions to the instationary Navier-Stokes system. In: Kaplicky, P., Necasova, S. (eds.) Topics on Partial Differential Equations, vol. 2, pp. 1–54. Publishing House of the Faculty of Mathematics and Physics Charles University, Prague (2007)
17. Freund, J., Stenberg, R.: On weakly imposed boundary conditions for second order problems. In: Proceedings of the International Conference on Finite Elements in Fluids, pp. 327–336 (1995)
18. Gunzburger, M., Kunoth, A.: Space-time adaptive wavelet methods for optimal control problems constrained by parabolic evolution equation. SIAM J. Control Optim. **49**(3), 1150–1170 (2011)
19. Héas, P., Mémin, E., Papadakis, N., Szantai, A.: Layered estimation of atmospheric mesoscale dynamics from satellite imagery. IEEE Trans. Geosci. Remote Sens. **45**(12), 4087–4104 (2007)
20. Heitz, D., Memin, E., Schnörr, C.: Variational fluid flow measurements from image sequences: synopsis and perspectives. Exp. Fluids. Published Online (2009)
21. Hesse, H.K., Kanschat, G.: Mesh adaptive multiple shooting for partial differential equations. Part I: linear quadratic optimal control problems. J. Numer. Math. **17**(3), 195–217 (2009)
22. Horn, B.K.P, Schunck, B.G.: Determining optical flow. Artif. Intell. **14**, 185–203 (1981)
23. Hou, L., Ravindran, S.: A penalized Neumann control approach for solving an optimal Dirichlet control problem for the Navier-Stokes equations. SIAM J. Control Optim. **36**(5), 1795–1814 (1998)
24. Juntunen, M., Stenberg, R.: Nitsche's method for general boundary conditions. Math. Comput. **78**(5), 1353–1373 (2009)
25. Klinger, M.: Parameter estimation problems in physically based image processing. In: Proceedings of ENUMATH 2011, pp. 191–199 (2013)
26. Kolmbauer, M., Langer, U.: Efficient solvers for some classes of time-periodic eddy current optimal control problems. In: Numerical Solution of Partial Differential Equations: Theory, Algorithms, and Their Applications, Springer, New York, pp. 203–216 (2013)
27. May, S., Rannacher, R., Vexler, B.: A priori error analysis for the finite element approximation of elliptic Dirichlet boundary control problems. In: Proceedings of ENUMATH 2007, pp. 637–644 (2007)
28. Meidner, D.: Adaptive space-time finite element methods for optimization problems governed by nonlinear parabolic systems. Ph.D. thesis, Heidelberg University (2008)
29. Nakajima, Y., Inomata, H., Nogawa, H., Sato, Y., Tamura, S., Okazaki, K., Torii, S.: Physics-based flow estimation of fluids. Pattern Recogn. **36**, 1203–1212 (2003)
30. Nitsche, J.: Über ein Variationsprinzip zur Lösung von Dirichlet-problemen bei Verwendung von Teilräumen, die keinen Randbedingungen unterworfen sind. Abhandlungen aus dem Mathematischen Seminar der Universität Hamburg **36**, 9–15 (1971)
31. Of, G., Phan, T., Steinbach, O.: An energy space finite elliptic Dirichlet boundary control problem. SFB-Report No. 2009-001, Uni Graz (2012)
32. Papadakis, N., Mémin, E.: Variational assimilation of fluid motion from image sequences. SIAM J. Image Sci. **1**(4), 343–363 (2008)

33. Pearson, J., Stoll, M.: Fast iterative solution of reaction-diffusion control problems arising from chemical processes. SIAM **35**(5), 987–1009 (2013)
34. Potschka, A.: A Direct Method for the Numerical Solution of Optimization Problems with Time-Periodic PDE Constraints. Springer, Berlin (2014)
35. Ruhnau, P.: Variational fluid motion estimation with physical priors. Ph.D. thesis, Mannheim University (2006)
36. Ruhnau, P., Schnörr, C.: Optical Stokes flow estimation: an imaging-based control approach. Exp. Fluids **42**, 61–78 (2007)
37. Ruhnau, P., Stahl, A., Schnörr, C.: Variational estimation of experimental fluid flows with physics-based spatio-temporal regularization. Meas. Sci. Technol. **18**(3), 755–763 (2007)
38. Stoll, M., Wathen, A.: All-at-once solution of time-dependent Stokes control. J. Comput. Phys. **232**, 498–515 (2013)
39. Temam, R.: Navier-Stokes Equations. AMS Chelsea Edition, North-Holland (1977)
40. Weiss, R.: The convergence of shooting methods. BIT **13**, 470–475 (1973)